Lifetime and production rate of beauty baryons from Z decays

P. Abreu, W. Adam, T. Adye, E. Agasi, I. Ajinenko, R. Aleksan, G D. Alekseev, P P. Allport, S. Almehed, S J. Alvsvaag, et al.

EUROPEAN ORGANIZATION FOR NUCLEAR RESEARCH

CERN–PPE/95–54

21 April 1995

Lifetime and production rate of beauty baryons from Z decays

DELPHI Collaboration

Abstract

The production and decay of beauty baryons (b-baryons) have been studied using 1.7×10^6 Z hadronic decays collected by the DELPHI detector at LEP. Three different techniques were used to identify the b-baryons. The first method used pairs of a Λ and a lepton to tag the b-baryon decay. The second method associated fully reconstructed Λ_c baryons with leptons. The third analysis reconstructed the b-baryon decay points by forming secondary vertices from identified protons and muons of opposite sign. Using these methods the following production rates were measured:

$$\begin{aligned} f(\mathrm{b} \to b\text{-baryon}) \times \mathrm{BR}(b\text{-baryon} \to \Lambda_s \ell \bar{\nu}_\ell \mathrm{X}) &= (0.30 \pm 0.06 \pm 0.04)\%, \\ f(\mathrm{b} \to b\text{-baryon}) \times \mathrm{BR}(b\text{-baryon} \to \Lambda_c \ell \bar{\nu}_\ell \mathrm{X}) &= (1.18 \pm 0.26^{+0.31}_{-0.21})\%, \\ f(\mathrm{b} \to b\text{-baryon}) \times \mathrm{BR}(b\text{-baryon} \to \mathrm{p} \mu \bar{\nu}_\mu \mathrm{X}) &= (0.49 \pm 0.11 \pm^{+0.15}_{-0.11})\%. \end{aligned}$$

The average b-baryon lifetime was determined to be:

$$\tau = 1.21^{+.21}_{-.18}(stat.) \pm 0.04(exp.syst.)^{+.02}_{-.07}(th.syst.) \text{ ps}.$$

(To be submitted to Zeit. f. Physik C)

P.Abreu[21], W.Adam[50], T.Adye[37], E.Agasi[31], I.Ajinenko[42], R.Aleksan[39], G.D.Alekseev[16], P.P.Allport[22], S.Almehed[24], S.J.Alvsvaag[4], U.Amaldi[9], S.Amato[47], A.Andreazza[28], M.L.Andrieux[14], P.Antilogus[25], W-D.Apel[17], Y.Arnoud[39], B.Åsman[44], J-E.Augustin[19], A.Augustinus[31], P.Baillon[9], P.Bambade[19], F.Barao[21], R.Barate[14], G.Barbiellini[46], D.Y.Bardin[16], G.J.Barker[35], A.Baroncelli[40], O.Barring[24], J.A.Barrio[26], W.Bartl[50], M.J.Bates[37], M.Battaglia[15], M.Baubillier[23], J.Baudot[39], K-H.Becks[52], M.Begalli[6], P.Beilliere[8], Yu.Belokopytov[9], A.C.Benvenuti[5], M.Berggren[41], D.Bertrand[2], F.Bianchi[45], M.Bigi[45], M.S.Bilenky[16], P.Billoir[23], D.Bloch[10], M.Blume[52], S.Blyth[35], V.Bocci[38], T.Bolognese[39], M.Bonesini[28], W.Bonivento[28], P.S.L.Booth[22], G.Borisov[42], C.Bosio[40], S.Bosworth[35], O.Botner[48], B.Bouquet[19], C.Bourdarios[9], T.J.V.Bowcock[22], M.Bozzo[13], P.Branchini[40], K.D.Brand[36], R.A.Brenner[15], C.Bricman[2], L.Brillault[23], R.C.A.Brown[9], P.Bruckman[18], J-M.Brunet[8], L.Bugge[33], T.Buran[33], A.Buys[9], M.Caccia[28], M.Calvi[28], A.J.Camacho Rozas[41], T.Camporesi[9], V.Canale[38], M.Canepa[13], K.Cankocak[44], F.Cao[2], F.Carena[9], P.Carrilho[47], L.Carroll[22], C.Caso[13], M.V.Castillo Gimenez[49], A.Cattai[9], F.R.Cavallo[5], L.Cerrito[38], V.Chabaud[9], M.Chapkin[42], Ph.Charpentier[9], L.Chaussard[25], J.Chauveau[23], P.Checchia[36], G.A.Chelkov[16], R.Chierici[45], P.Chliapnikov[42], P.Chochula[7], V.Chorowicz[9], V.Cindro[43], P.Collins[9], J.L.Contreras[19], R.Contri[13], E.Cortina[49], G.Cosme[19], F.Cossutti[46], H.B.Crawley[1], D.Crennell[37], G.Crosetti[13], J.Cuevas Maestro[34], S.Czellar[15], E.Dahl-Jensen[29], J.Dahm[52], B.Dalmagne[19], M.Dam[33], G.Damgaard[29], A.Daum[17], P.D.Dauncey[37], M.Davenport[9], W.Da Silva[23], C.Defoix[8], G.Della Ricca[46], P.Delpierre[27], N.Demaria[35], A.De Angelis[9], H.De Boeck[2], W.De Boer[17], S.De Brabandere[2], C.De Clercq[2], C.De La Vaissiere[23], B.De Lotto[46], A.De Min[28], L.De Paula[47], C.De Saint-Jean[39], H.Dijkstra[9], L.Di Ciaccio[38], F.Djama[10], J.Dolbeau[8], M.Donszelmann[9], K.Doroba[51], M.Dracos[10], J.Drees[52], K.-A.Drees[52], M.Dris[32], Y.Dufour[8], F.Dupont[14], D.Edsall[1], R.Ehret[17], G.Eigen[4], T.Ekelof[48], G.Ekspong[44], M.Elsing[52], J-P.Engel[10], N.Ershaidat[23], B.Erzen[43], M.Espirito Santo[21], E.Falk[24], D.Fassouliotis[32], M.Feindt[9], A.Fenyuk[42], A.Ferrer[49], T.A.Filippas[32], A.Firestone[1], H.Foeth[9], E.Fokitis[32], F.Fontanelli[13], F.Formenti[9], B.Franek[37], P.Frenkiel[8], D.C.Fries[17], A.G.Frodesen[4], R.Fruhwirth[50], F.Fulda-Quenzer[19], H.Furstenau[9], J.Fuster[49], A.Galloni[22], D.Gamba[45], M.Gandelman[6], C.Garcia[49], J.Garcia[41], C.Gaspar[9], U.Gasparini[36], Ph.Gavillet[9], E.N.Gazis[32], D.Gele[10], J-P.Gerber[10], M.Gibbs[22], D.Gillespie[9], R.Gokieli[51], B.Golob[43], G.Gopal[37], L.Gorn[1], M.Gorski[51], V.Gracco[13], E.Graziani[40], G.Grosdidier[19], P.Gunnarsson[44], M.Gunther[48], J.Guy[37], U.Haedinger[17], F.Hahn[52], M.Hahn[17], S.Hahn[52], Z.Hajduk[18], A.Hallgren[48], K.Hamacher[52], W.Hao[31], F.J.Harris[35], V.Hedberg[24], R.Henriques[21], J.J.Hernandez[49], P.Herquet[2], H.Herr[9], T.L.Hessing[9], E.Higon[49], H.J.Hilke[9], T.S.Hill[1], S-O.Holmgren[44], P.J.Holt[35], D.Holthuizen[31], M.Houlden[22], J.Hrubec[50], K.Huet[2], K.Hultqvist[44], P.Ioannou[3], J.N.Jackson[22], R.Jacobsson[44], P.Jalocha[18], R.Janik[7], G.Jarlskog[24], P.Jarry[39], B.Jean-Marie[19], E.K.Johansson[44], L.Jonsson[24], P.Jonsson[24], C.Joram[9], P.Juillot[10], M.Kaiser[17], G.Kalmus[37], F.Kapusta[23], M.Karlsson[44], E.Karvelas[11], S.Katsanevas[3], E.C.Katsoufis[32], R.Keranen[15], B.A.Khomenko[16], N.N.Khovanski[16], B.King[22], N.J.Kjaer[29], H.Klein[9], A.Klovning[4], P.Kluit[31], J.H.Koehne[17], B.Koene[31], P.Kokkinias[11], M.Koratzinos[9], V.Kostioukhine[42], C.Kourkoumelis[3], O.Kouznetsov[13], P.-H.Kramer[52], M.Krammer[50], C.Kreuter[17], J.Krolikowski[51], I.Kronkvist[24], Z.Krumstein[16], W.Krupinski[18], P.Kubinec[7], W.Kucewicz[18], K.Kurvinen[15], C.Lacasta[49], I.Laktineh[25], S.Lamblot[23], J.W.Lamsa[1], L.Lanceri[46], D.W.Lane[1], P.Langefeld[52], V.Lapin[42], I.Last[22], J-P.Laugier[39], R.Lauhakangas[15], G.Leder[50], F.Ledroit[14], V.Lefebure[2], C.K.Legan[1], R.Leitner[30], Y.Lemoigne[39], J.Lemonne[2], G.Lenzen[52], V.Lepeltier[19], T.Lesiak[36], D.Liko[50], R.Lindner[52], A.Lipniacka[19], I.Lippi[36], B.Loerstad[24], M.Lokajicek[12], J.G.Loken[35], J.M.Lopez[41], A.Lopez-Fernandez[9], M.A.Lopez Aguera[41], D.Loukas[11], P.Lutz[39], L.Lyons[35], J.MacNaughton[50], G.Maehlum[17], A.Maio[21], V.Malychev[16], F.Mandl[50], J.Marco[41], B.Marechal[47], M.Margoni[36], J-C.Marin[9], C.Mariotti[40], A.Markou[11], T.Maron[52], C.Martinez-Rivero[41], F.Martinez-Vidal[49], S.Marti i Garcia[49], F.Matorras[41], C.Matteuzzi[28], G.Matthiae[38], M.Mazzucato[36], M.Mc Cubbin[9], R.Mc Kay[1], R.Mc Nulty[22], J.Medbo[48], C.Meroni[28], W.T.Meyer[1], M.Michelotto[36], E.Migliore[45], L.Mirabito[25], W.A.Mitaroff[50], U.Mjoernmark[24], T.Moa[44], R.Moeller[29], K.Moenig[9], M.R.Monge[13], P.Morettini[13], H.Mueller[17], L.M.Mundim[6], W.J.Murray[37], B.Muryn[18], G.Myatt[35], F.Naraghi[14], F.L.Navarria[5], S.Navas[49], P.Negri[28], S.Nemecek[12], W.Neumann[52], N.Neumeister[50], R.Nicolaidou[3], B.S.Nielsen[29], M.Nieuwenhuizen[31], V.Nikolaenko[10], P.Niss[44], A.Nomerotski[36], A.Normand[35], W.Oberschulte-Beckmann[17], V.Obraztsov[42], A.G.Olshevski[16], A.Onofre[21], R.Orava[15], A.Ostankov[42], K.Osterberg[15], A.Ouraou[39], P.Paganini[19], M.Paganoni[28], P.Pages[10], H.Palka[18], Th.D.Papadopoulou[32], L.Pape[9], C.Parkes[35], F.Parodi[13], A.Passeri[40], M.Pegoraro[36], L.Peralta[21], H.Pernegger[50], M.Pernicka[50], A.Perrotta[5], C.Petridou[46], A.Petrolini[13], H.T.Phillips[37], G.Piana[13], F.Pierre[39], S.Plaszczynski[19], O.Podobrin[17], M.E.Pol[6], G.Polok[18], P.Poropat[46], V.Pozdniakov[16], M.Prest[46], P.Privitera[38], N.Pukhaeva[16], A.Pullia[28], D.Radojicic[35], S.Ragazzi[28], H.Rahmani[32], J.Rames[12], P.N.Ratoff[20], A.L.Read[33], M.Reale[52], P.Rebecchi[19], N.G.Redaelli[28], D.Reid[9], P.B.Renton[35], L.K.Resvanis[3], F.Richard[19], J.Richardson[22], J.Ridky[12], G.Rinaudo[45], I.Ripp[39], A.Romero[45], I.Roncagliolo[13], P.Ronchese[36], L.Roos[14], E.I.Rosenberg[1], E.Rosso[9], P.Roudeau[19], T.Rovelli[5], W.Ruckstuhl[31], V.Ruhlmann-Kleider[39], A.Ruiz[41], K.Rybicki[18], H.Saarikko[15], Y.Sacquin[39], A.Sadovsky[16], G.Sajot[14], J.Salt[49], J.Sanchez[26], M.Sannino[13], H.Schneider[17], M.A.E.Schyns[52], G.Sciolla[45], F.Scuri[46], Y.Sedykh[16], A.M.Segar[35],

A.Seitz[17], R.Sekulin[37], R.C.Shellard[6], I.Siccama[31], P.Siegrist[39], S.Simonetti[39], F.Simonetto[36], A.N.Sisakian[16], B.Sitar[7], T.B.Skaali[33], G.Smadja[25], N.Smirnov[42], O.Smirnova[16], G.R.Smith[37], R.Sosnowski[51], D.Souza-Santos[6], T.Spassov[21], E.Spiriti[40], S.Squarcia[13], H.Staeck[52], C.Stanescu[40], S.Stapnes[33], I.Stavitski[36], K.Stepaniak[51], F.Stichelbaut[9], A.Stocchi[19], J.Strauss[50], R.Strub[10], B.Stugu[4], M.Szczekowski[51], M.Szeptycka[51], T.Tabarelli[28], J.P.Tavernet[23], O.Tchikilev[42], A.Tilquin[27], J.Timmermans[31], L.G.Tkatchev[16], T.Todorov[10], D.Z.Toet[31], A.Tomaradze[2], B.Tome[21], E.Torassa[45], L.Tortora[40], G.Transtromer[24], D.Treille[9], W.Trischuk[9], G.Tristram[8], A.Trombini[19], C.Troncon[28], A.Tsirou[9], M-L.Turluer[39], I.A.Tyapkin[16], M.Tyndel[37], S.Tzamarias[22], B.Ueberschaer[52], S.Ueberschaer[52], O.Ullaland[9], V.Uvarov[42], G.Valenti[5], E.Vallazza[9], G.W.Van Apeldoorn[31], P.Van Dam[31], W.K.Van Doninck[2], J.Van Eldik[31], N.Vassilopoulos[35], G.Vegni[28], L.Ventura[36], W.Venus[37], F.Verbeure[2], M.Verlato[36], L.S.Vertogradov[16], D.Vilanova[39], P.Vincent[25], L.Vitale[46], E.Vlasov[42], A.S.Vodopyanov[16], V.Vrba[12], H.Wahlen[52], C.Walck[44], A.Wehr[52], M.Weierstall[52], P.Weilhammer[9], A.M.Wetherell[9], D.Wicke[52], J.H.Wickens[2], M.Wielers[17], G.R.Wilkinson[35], W.S.C.Williams[35], M.Winter[10], M.Witek[9], G.Wormser[19], K.Woschnagg[48], K.Yip[35], F.Zach[25], C.Zacharatou[24], A.Zaitsev[42], A.Zalewska[18], P.Zalewski[51], D.Zavrtanik[43], E.Zevgolatakos[11], N.I.Zimin[16], M.Zito[39], D.Zontar[43], R.Zuberi[35], G.C.Zucchelli[44], G.Zumerle[36]

[1] Ames Laboratory and Department of Physics, Iowa State University, Ames IA 50011, USA
[2] Physics Department, Univ. Instelling Antwerpen, Universiteitsplein 1, B-2610 Wilrijk, Belgium
and IIHE, ULB-VUB, Pleinlaan 2, B-1050 Brussels, Belgium
and Faculté des Sciences, Univ. de l'Etat Mons, Av. Maistriau 19, B-7000 Mons, Belgium
[3] Physics Laboratory, University of Athens, Solonos Str. 104, GR-10680 Athens, Greece
[4] Department of Physics, University of Bergen, Allégaten 55, N-5007 Bergen, Norway
[5] Dipartimento di Fisica, Università di Bologna and INFN, Via Irnerio 46, I-40126 Bologna, Italy
[6] Centro Brasileiro de Pesquisas Físicas, rua Xavier Sigaud 150, RJ-22290 Rio de Janeiro, Brazil
and Depto. de Física, Pont. Univ. Católica, C.P. 38071 RJ-22453 Rio de Janeiro, Brazil
and Inst. de Física, Univ. Estadual do Rio de Janeiro, rua São Francisco Xavier 524, Rio de Janeiro, Brazil
[7] Comenius University, Faculty of Mathematics and Physics, Mlynska Dolina, SK-84215 Bratislava, Slovakia
[8] Collège de France, Lab. de Physique Corpusculaire, IN2P3-CNRS, F-75231 Paris Cedex 05, France
[9] CERN, CH-1211 Geneva 23, Switzerland
[10] Centre de Recherche Nucléaire, IN2P3 - CNRS/ULP - BP20, F-67037 Strasbourg Cedex, France
[11] Institute of Nuclear Physics, N.C.S.R. Demokritos, P.O. Box 60228, GR-15310 Athens, Greece
[12] FZU, Inst. of Physics of the C.A.S. High Energy Physics Division, Na Slovance 2, 180 40, Praha 8, Czech Republic
[13] Dipartimento di Fisica, Università di Genova and INFN, Via Dodecaneso 33, I-16146 Genova, Italy
[14] Institut des Sciences Nucléaires, IN2P3-CNRS, Université de Grenoble 1, F-38026 Grenoble Cedex, France
[15] Research Institute for High Energy Physics, SEFT, P.O. Box 9, FIN-00014 Helsinki, Finland
[16] Joint Institute for Nuclear Research, Dubna, Head Post Office, P.O. Box 79, 101 000 Moscow, Russian Federation
[17] Institut für Experimentelle Kernphysik, Universität Karlsruhe, Postfach 6980, D-76128 Karlsruhe, Germany
[18] High Energy Physics Laboratory, Institute of Nuclear Physics, Ul. Kawiory 26a, PL-30055 Krakow 30, Poland
[19] Université de Paris-Sud, Lab. de l'Accélérateur Linéaire, IN2P3-CNRS, Bat 200, F-91405 Orsay Cedex, France
[20] School of Physics and Materials, University of Lancaster, Lancaster LA1 4YB, UK
[21] LIP, IST, FCUL - Av. Elias Garcia, 14-1°, P-1000 Lisboa Codex, Portugal
[22] Department of Physics, University of Liverpool, P.O. Box 147, Liverpool L69 3BX, UK
[23] LPNHE, IN2P3-CNRS, Universités Paris VI et VII, Tour 33 (RdC), 4 place Jussieu, F-75252 Paris Cedex 05, France
[24] Department of Physics, University of Lund, Sölvegatan 14, S-22363 Lund, Sweden
[25] Université Claude Bernard de Lyon, IPNL, IN2P3-CNRS, F-69622 Villeurbanne Cedex, France
[26] Universidad Complutense, Avda. Complutense s/n, E-28040 Madrid, Spain
[27] Univ. d'Aix - Marseille II - CPP, IN2P3-CNRS, F-13288 Marseille Cedex 09, France
[28] Dipartimento di Fisica, Università di Milano and INFN, Via Celoria 16, I-20133 Milan, Italy
[29] Niels Bohr Institute, Blegdamsvej 17, DK-2100 Copenhagen 0, Denmark
[30] NC, Nuclear Centre of MFF, Charles University, Areal MFF, V Holesovickach 2, 180 00, Praha 8, Czech Republic
[31] NIKHEF-H, Postbus 41882, NL-1009 DB Amsterdam, The Netherlands
[32] National Technical University, Physics Department, Zografou Campus, GR-15773 Athens, Greece
[33] Physics Department, University of Oslo, Blindern, N-1000 Oslo 3, Norway
[34] Dpto. Fisica, Univ. Oviedo, C/P. Pérez Casas, S/N-33006 Oviedo, Spain
[35] Department of Physics, University of Oxford, Keble Road, Oxford OX1 3RH, UK
[36] Dipartimento di Fisica, Università di Padova and INFN, Via Marzolo 8, I-35131 Padua, Italy
[37] Rutherford Appleton Laboratory, Chilton, Didcot OX11 OQX, UK
[38] Dipartimento di Fisica, Università di Roma II and INFN, Tor Vergata, I-00173 Rome, Italy
[39] Centre d'Etude de Saclay, DSM/DAPNIA, F-91191 Gif-sur-Yvette Cedex, France
[40] Istituto Superiore di Sanità, Ist. Naz. di Fisica Nucl. (INFN), Viale Regina Elena 299, I-00161 Rome, Italy
[41] C.E.A.F.M., C.S.I.C. - Univ. Cantabria, Avda. los Castros, S/N-39006 Santander, Spain, (CICYT-AEN93-0832)
[42] Inst. for High Energy Physics, Serpukov P.O. Box 35, Protvino, (Moscow Region), Russian Federation
[43] J. Stefan Institute and Department of Physics, University of Ljubljana, Jamova 39, SI-61000 Ljubljana, Slovenia
[44] Fysikum, Stockholm University, Box 6730, S-113 85 Stockholm, Sweden
[45] Dipartimento di Fisica Sperimentale, Università di Torino and INFN, Via P. Giuria 1, I-10125 Turin, Italy
[46] Dipartimento di Fisica, Università di Trieste and INFN, Via A. Valerio 2, I-34127 Trieste, Italy
and Istituto di Fisica, Università di Udine, I-33100 Udine, Italy
[47] Univ. Federal do Rio de Janeiro, C.P. 68528 Cidade Univ., Ilha do Fundão BR-21945-970 Rio de Janeiro, Brazil
[48] Department of Radiation Sciences, University of Uppsala, P.O. Box 535, S-751 21 Uppsala, Sweden
[49] IFIC, Valencia-CSIC, and D.F.A.M.N., U. de Valencia, Avda. Dr. Moliner 50, E-46100 Burjassot (Valencia), Spain
[50] Institut für Hochenergiephysik, Österr. Akad. d. Wissensch., Nikolsdorfergasse 18, A-1050 Vienna, Austria
[51] Inst. Nuclear Studies and University of Warsaw, Ul. Hoza 69, PL-00681 Warsaw, Poland
[52] Fachbereich Physik, University of Wuppertal, Postfach 100 127, D-42097 Wuppertal 1, Germany

1 Introduction

The Λ_b baryon was first observed in the exclusive decay $\Lambda_b \to \Lambda J/\psi$ by the UA1 experiment at the $Sp\bar{p}S$ collider [1]. Evidence for its production in Z hadronic decays has been reported by the LEP experiments [2,3]. They attributed the observed correlation between Λ's and leptons (ℓ's) to Λ_b decays. Measurements of the average b-baryon lifetime have been recently published [3,4]. Its precise determination tests the theory of heavy quark decays and the simple quark-spectator model. This is of particular interest for the beauty quark [5] where, due to the high b-quark mass, the theoretical predictions based on perturbative expansions are less uncertain than those for charm decays.

This paper extends the previous analysis [3] and adds two new semileptonic decay channels, based on the detection of a Λ_c or a fast proton (p) in the same jet as a high transverse momentum lepton. The $\Lambda\ell$ channel provides a clear signature for b-baryon production but the position of the b-baryon decay vertex is precisely determined with relatively low efficiency. The $\Lambda_c\ell$ channel provides the purest b-baryon sample. Finally the $p\ell$ channel relies on the particle identification capabilities of DELPHI.

2 The DELPHI Detector

The DELPHI detector has been described in detail elsewhere [6]. Both charged particle tracking through the uniform axial field and particle identification are important in this analysis. The detector elements used for tracking are: the Vertex Detector (VD), the Inner Detector (ID), the Time Projection Chamber (TPC) and the Outer Detector (OD). The other important detectors are: the the Ring Imaging Cherenkov detector (RICH) for hadron identification, the barrel electromagnetic calorimeter (HPC) and the muon chambers for lepton identification. The ionization loss dE/dx measurements in the TPC are also used for particle identification.

The VD, consisting of 3 cylindrical layers of silicon detectors (radii 6, 8 and 11 cm), provides up to 3 hits per track (or more in small overlapping regions) in the polar angle range $43^o < \theta < 137^o$. The intrinsic resolution of the VD points is $\pm 8\mu$m, measured only in the plane transverse to the beam direction ($r\phi$ plane). The precision on the impact parameter with respect to the primary vertex of a track having hits associated in the VD is $\pm 26\mu$m, measured in dimuon Z events.

Charged particle tracks were reconstructed with 95% efficiency and with a momentum resolution $\sigma_p/p < 2.0 \times 10^{-3} p$ (GeV/c). The primary vertex of the e^+e^- interaction was reconstructed on an event-by-event basis using a beam spot constraint. The position of the primary vertex could be determined in this way to a precision of about $40\mu m$ (slightly dependent on the flavour of the primary quark-antiquark pair) in the plane transverse to the beam direction. In this plane secondary vertices from beauty and charm decays were reconstructed with a precision of $\pm 300\mu$m along the flight direction of the decaying particles. The $\Lambda \to p\pi$ decays could be reconstructed if the distance (in the $r\phi$ plane) between the Λ decay point and primary vertex was less than 90 cm. This condition meant that the proton and pion had track segments at least 20 cm long in the TPC.

Hadron identification relied on the specific ionization in the TPC and on the RICH detector. The dE/dx measurement had a precision of $\pm 7\%$ in the momentum range $4 < p < 25$ GeV/c. The RICH detector [7] consisted of a liquid radiator which provided $p/K/\pi$ separation in the intermediate momentum region 2–8 GeV/c, and a gas radiator which worked in veto mode for proton selection in the region 8–15 GeV/c and separated protons from kaons for momenta less than 30 GeV/c.

The barrel electromagnetic calorimeter (HPC), covered the polar angle region $46° < \theta < 134°$, and detected electrons with an energy precision $\sigma_E/E = 0.25/\sqrt{E}(GeV)$.

Two planes of muon chambers covered the polar angle region $20° < \theta < 160°$, except for two regions of $\pm 3°$ around $\theta = 42°$ and $\theta = 138°$. The first layer was inside the return yoke of the magnet, after 90 cm of iron, while the second was mounted outside the yoke, behind a further 20 cm of iron.

3 Lepton selection and hadron identification

Hadronic events from Z decays were selected by requiring a charged multiplicity greater than 4 and a total reconstructed energy greater than 0.12 $\sqrt{s}$; charged particles were required to have a momentum greater than 0.4 GeV/c and polar angle between 20^o and 160^o. The overall trigger and selection efficiency was 0.950 ± 0.011 [8]. Lepton candidates in these events were used in the analysis if their momentum was greater than 3 GeV/c.

3.1 Electron Identification

The probability of any track being due to an electron was calculated using the spatial separation between the extrapolated position of a track at the HPC and the position of the nearest electro-magnetic shower, a match between the measured energy and the track momentum and a successful fit to the longitudinal profile of the shower in the 9 HPC layers [9]. Tracks with a χ^2 probability greater than 4% for this electron hypothesis were retained for further analysis. The final electron sample was obtained by using additional information from the TPC and RICH. The dE/dx measurement in the TPC was used to check that the specific ionization for the track was consistent with that expected from electrons with a probability of at least 2%. Also, when the gas RICH was sensitive it was required to show at least one associated photoelectron at the correct angle for the electron hypothesis. Electrons arising from photon conversions were removed by a vertex fit to pairs of electron candidates. If the e^+e^- invariant mass was reconstructed to be less than 20 MeV/c^2 the pair was assumed to be a converted photon. Using this procedure the electron identification efficiency in the HPC fiducial volume was found to be $(62 \pm 1)\%$, with a hadron misidentification probability of $(1.5 \pm 0.4)\%$.

3.2 Muon Identification

The identification of muons relied on the muon chambers. Tracks were extrapolated to the muon chambers and a global χ^2 of the track was used to define a refitting procedure which took into account the multiple scattering between the inner tracking devices and the muon chambers. At least 1 hit in the chamber layer outside the iron yoke and a $\chi^2/ndof < 5$ were required (< 6 in the forward region). The corresponding muon identification efficiency was $(81 \pm 1)\%$ in the barrel and $(82 \pm 2)\%$ in the end-caps, with hadron misidentification probabilities of $(1.01 \pm 0.05)\%$ and $(1.15 \pm 0.08)\%$ respectively.

3.3 Hadron Identification using the RICH

Particle identification using the DELPHI RICH detector has been described in detail elsewhere [10]. The three analyses presented in this paper used protons with momentum range well above the pion threshold in the gas radiator of 2.5 GeV/c. Above this threshold, the gas radiator worked in veto-mode for p/π separation up to 16 GeV/c, with 75%

efficiency and a pion rejection factor of 15. A K/p separation with the same background rejection power was ensured in this mode of operation between 8.5 GeV/c, the gas radiator threshold for kaons, and 16 GeV/c. Above this energy, identification was provided by the measurement of the Cherenkov angle of the detected photons using a "ring identification mode" algorithm [10], with 80% efficiency and rejection factors 5-10. This algorithm was also applied to the liquid radiator data, which provided complementary information for K/π and K/p separation in the momentum range 1-7 GeV/c. The RICH was operational for 25% of the 1991 data, 60% of the 1992 data and nearly 90% of the 1993 data sample (gas radiator only).

4 $\Lambda\ell$ Channel

The analysis of events with a Λ and a lepton is based on about 1.7×10^6 Z hadronic decays collected in the years 1991 - 1993. Decays of b-baryons with a $\Lambda\ell$ pair in the final state originate mainly from the decay chain: b-baryon $\to \Lambda_c \ell \nu X, \Lambda_c \to \Lambda X$. These decays have the following properties: the lepton has high transverse and longitudinal momentum, the Λ has a harder momentum spectrum than the Λ produced in light quark fragmentation and the $\Lambda\ell$ pair has the *right sign* i.e. $p\ell^-$ rather than $p\ell^+$, where p is the proton from the Λ decay. In the following the lepton transverse momentum (p_T) is computed, if not otherwise stated, with respect to the jet axis defined including the lepton in the jet. Charged particles are clustered into jets using the LUND jet finding algorithm [11] (routine LUCLUS) with a clustering mass parameter equal to 2.5 GeV/c^2.

Semileptonic B meson decays, such as $B \to \Lambda_c \bar{N} \ell^- \nu X$ (where $\bar{N}$ is an antibaryon), can also contribute to an excess in right sign pairs. This was estimated to be negligible, under the conservative assumption that 100% of b quarks hadronize to a B meson, using the 90% CL upper limit $BR(\bar{B} \to p\ell^-\nu X) < 1.6\ 10^{-3}$ [12] and the CLEO result that 30% of the protons produced in B decays come from Λ particles [13]. This conclusion takes into account the fact that the efficiency of the selection cuts described below (section 4.2) for this channel is smaller by a factor 3 than for the b-baryon decay.

Background events from direct c-quark production through the $c \to \Lambda_c \to \Lambda\ell\nu X$ decay chain have protons and the leptons of the same sign; in addition, the lepton p_T spectrum is softer. A quantitative analysis of the background based on detailed simulation of Z hadronic events is discussed in section 4.3.

4.1 Λ selection

In the search for $\Lambda \to p\pi$ decay all pairs of opposite sign charged particles with momentum $0.1 < p < 30$ GeV/c were considered. A candidate Λ vertex was formed if the minimum separation in the $r\phi$ plane of the two tracks was less than 3 mm and if their perigee separation in the beam direction was less than 5 mm. If the same track was associated with more than one vertex only the vertex with the largest decay length (in the $r\phi$ projection) was used. For decays inside the beam pipe at least one vertex detector hit was required per track. Only combinations where the vertex was closer to the primary vertex than the starting point of both tracks were kept.

Particle identification greatly improved the background rejection with negligible loss in efficiency. The identification criteria using the dE/dx measurement in the TPC and the selections for rejection of γ conversions and K^0 decays are described previously [3]. If the extrapolation of the track of charged particle with highest momentum (assumed to be the proton) to the RICH was in the sensitive volume of the detector and the RICH was

operational, the identification algorithm described in section 3.3 was used. To improve the signal-to-noise ratio further, the following kinematic selection criteria were applied: the angle in the $r\phi$ plane between the line of flight and the reconstructed Λ momentum was required to be smaller than 2° and the probability for the lifetime of the Λ decay candidate to be greater than that observed was required to be greater than 4%.

Figure 1a shows the pπ invariant mass distribution for the remaining candidates with momentum greater than 4 GeV/c. In this sample the fitted Λ signal was 22793 ± 556 decays, with a Λ mass mean value of 1114.9 ± 0.1 MeV/c^2 and a measured width of 4.1 ± 0.6 MeV/c^2.

The momentum distribution for the reconstructed Λ candidates with the background subtracted is shown in figure 1.b for the mass range from 1106 to 1126 MeV/c^2. It is compared with the prediction of the DELPHI simulation program using the JETSET 7.3 model [14] with the results analysed using the same programs as the real data. The $\Lambda \to p\pi$ reconstruction efficiency from the simulation, shown in figure 1c, was (20$\pm$1)% for $p > 4$ GeV/c. This increase in efficiency compared with the previous DELPHI publication [3] is due to improved pattern recognition.

4.2 $\Lambda\ell$ Correlations

To select Λ and leptons coming from the Λ_b decay chain, the following criteria were applied: the momentum of the Λ candidate was required to be greater than 4 GeV/c and the momentum of the lepton greater than 3 GeV/c. The lepton was only used if it was in the same jet as the Λ and its p_T was greater than 0.5 GeV/c. The mass of the $\Lambda\ell$ combination was required to lie in the range 1.9 to 5.0 GeV/c^2 and the $\Lambda\ell$ pairs were only selected for analysis if their total momentum was greater than 9 GeV/c. In the simulation the above procedure reduced background sources of $\Lambda\ell$ pairs by more than two orders of magnitude [3] and selected $\Lambda_b \to \Lambda\ell\nu X$ decays (provided the Λ was reconstructed) with an efficiency of (50 ± 3)%.

The $p\pi$ invariant mass spectra in the data for the right and wrong sign $\Lambda\ell$ pairs are shown by the dots in figures 2.a and 2.b, together with the result of a fit to the data using a Gaussian function and a polynomial background. The fit gives a signal of (234 ± 20) Λ's in the right sign pairs and (112 ± 19) Λ's in the wrong sign pairs. The histograms show the corresponding distributions from simulation normalized to the total number of hadronic Z events. The yield of genuine Λ's predicted by the simulation is shown by the single hatched area; the double hatched areas show the simulation prediction for the Λ coming from a b-baryon decay.

The simulation assumed a Λ_b production rate $f(b \to \Lambda_b) \times Br(\Lambda_b \to \Lambda\ell\nu X) = 0.3\%$ and a combined Ξ_b and Σ_b production rate of 0.03 %. It also predicted a small signal in the wrong sign pair combinations, due to $\Lambda_c \to \Lambda\ell\nu X$ decays and to the associated production of $\Lambda_b + \bar{\Lambda}$ in which the $\bar{\Lambda}$ was reconstructed and associated with the lepton.

4.3 Branching Ratios

As shown in figures 2.a,b, the simulation included a large number of Λ's coming from sources other than b-baryon decays, in both right and wrong sign combinations. The absolute value was model dependent and was not used in this analysis. However the ratio ($R = 1.0 \pm 0.1$) of the background level of Λ's in the two distributions in figures 2.a and 2.b was assumed to be correct. The statistical error of 0.1 on this ratio was

included in the systematic error on the production rate. Moreover, a small b-baryon signal ($15 \pm 5\%$ of the signal in the right sign sample) was predicted in the wrong sign pair sample. Thus, to estimate the b-baryon yield in the right sign sample, the Λ signal in wrong sign combinations was subtracted from the signal in figure 2a and the result scaled by the correction factor $C = 1/(0.85 \pm 0.05)$. This led to a total b-baryon signal of $144 \pm 33(stat.) \pm 14(syst.)$ events.

For the analysis of the $\Lambda\mu$ pairs, a hadronic data sample in which the TPC and the barrel and forward muon chambers were more than 90% operational was used. This selected 1,620,000 Z events. The overall efficiency for the $\Lambda\mu$ channel was $(4.4 \pm 0.4)\%$. The estimated number of b-baryons in this sample ($118 \pm 27 \pm 12$) leads to a production rate:

$$f(\mathrm{b} \to b\text{-baryon}) \times Br(b\text{-baryon} \to \Lambda\mu\nu X) = (0.36 \pm 0.07^{+0.05}_{-0.04})\%.$$

For the analysis of the Λe pairs, the hadronic data sample in which the TPC and HPC were more than 90% operational was used; this requirement selected 1,589,000 Z events. The overall efficiency for the Λe channel was $(2.0 \pm 0.3)\%$. The estimated number of b-baryons in the sample was ($26 \pm 19 \pm 3$), giving a production rate:

$$f(\mathrm{b} \to b\text{-baryon}) \times Br(b\text{-baryon} \to \Lambda e\nu X) = (0.18 \pm 0.12^{+0.03}_{-0.02})\%.$$

Assuming lepton universality, these results may be averaged to give:

$$f(\mathrm{b} \to b\text{-baryon}) \times Br(b\text{-baryon} \to \Lambda\ell\nu X) = (0.30 \pm 0.06 \pm 0.04)\%.$$

Table 1 shows the contributions from different sources to the total systematic uncertainty. The efficiency of the selection defined by the kinematic cuts discussed in section 4.2 was dependent on the momentum spectrum, the polarization and the decay model assumed for the b-baryon. The polarization value quoted in the table is the central one of the allowed range [-0.936, 0.0], where the lower limit is the Standard Model prediction for the polarization of the original b quark, assuming $sin^2\theta_W = 0.23$. The b-baryon semileptonic decay was simulated in the framework of Heavy Quark Effective Theory [15] using the following parameterization of the Isgur-Wise function:

$$\eta(\omega) = exp[a_{IW}(1-\omega)],$$

where $\omega = v_{\Lambda_b} \cdot v_{\Lambda_c}$ and v_{Λ_b} (v_{Λ_c}) is the b-baryon (c-baryon) 4-velocity. A further effect arose if resonant and non-resonant $\Lambda_b \to \Lambda_c n\pi\ell\nu$ decays were an important fraction of the total width, where n is a positive integer. Finally, different assumptions about the $\Lambda_c \to \Lambda X$ branching fractions gave negligible effects on the overall efficiency. As can be seen from the table, the dominant contribution to the systematic error comes from the background subtraction procedure used to eliminate accidental $\Lambda\ell$ correlations. The above result can be compared with the previous determination by DELPHI [3]: $f(b \to \Lambda_b) \times Br(\Lambda_b \to \Lambda\ell\nu X) = (0.41 \pm 0.13(stat.) \pm 0.09(syst.))\%$.

Figure 3a shows the right-sign Λ momentum spectrum after the subtraction of the wrong sign Λ sample for the data (dots); the superimposed histogram, showing the simulation prediction for the momentum of reconstructed Λ originating from a b-baryon, was in good agreement with the observed spectrum. Similar plots for the lepton p_T spectrum, the sum of the lepton and Λ momenta and the $\Lambda\ell$ invariant mass are shown in figures 3.b-d.

Table 1: Contributions to the total systematic uncertainty on the b-baryon production rate times its branching ratio to $\Lambda\ell\nu X$.

Source	variation level	Syst.uncertainty($\times 10^2$)
lepton identification efficiency	$\pm 2\%$	± 0.006
Λ reconstruction efficiency	0.20 ± 0.01	± 0.016
background subtraction	–	± 0.032
$< \mathrm{E_b} > / \mathrm{E_{beam}}$	0.70 ± 0.03	± 0.009
$\eta(\omega) = \exp[a_{IW}(1-\omega)]$	$a_{IW} = 1.7^{+3.3}_{-1.7}$	± 0.008
Λ_b polarization	-0.47 ± 0.47	± 0.013
$\mathrm{BR}(\Lambda_\mathrm{b} \to \Lambda_\mathrm{c}\ell\nu\mathrm{n}\pi)/\mathrm{BR}(\Lambda_\mathrm{b} \to \Lambda_\mathrm{c}\ell\nu)$	$0 \to 0.3$	$+0.020$
total syst. uncertainty	–	$^{+0.045}_{-0.040}$

4.4 Measurement of b-baryon lifetime

The analysis followed the method previously used [3] and was based on the muon sample only. Since the extrapolation of the Λ flight direction to the interaction region was not precise enough to separate secondary from tertiary vertices in the b-baryon decay chain, a unique secondary vertex was reconstructed using the Λ, the correlated high p_T muon and an oppositely charged particle (assumed to be a pion) with momentum greater than 0.4 GeV/c . The muon and the candidate pion were required to have at least 2 associated hits in the microvertex detector. To reduce the combinatorial background, the $(\mu\Lambda\pi)$ invariant mass was required to be less than 5.6 GeV/c^2 and the $(\Lambda\pi)$ invariant mass to be less than 2.4 GeV/c^2. Furthermore, the contribution of the muon and pion track to the χ^2 of the vertex was required to be less than 3.5 and the contribution of the Λ flight path less than 5. In case of more than one reconstructed vertex, the vertex with the pion of highest momentum was chosen. Out of 240 right sign $\Lambda\mu$ events with $1.106 < M(p\pi) < 1.126$ GeV/c^2, 63 decay vertices were reconstructed.

This procedure selected b-baryons in which the subsequent charmed particle in the decay chain had a small decay length with respect to the resolution of secondary vertices. In simulated data this did not introduce any sizeable bias in the decay length distribution of the b-baryon; the efficiency was 40%, and in 90% of the cases the candidate pion associated with the vertex originated from the Λ_b decay chain.

The b-baryon purity of the sample after the vertex reconstruction, F_s, was determined from the data by a fit to the mass plots for the right and wrong sign correlations (figures 4.a,b). Assuming an equal number of background events in both samples, the fit gave $F_s = (61 \pm 7)\%$.

Background events came from fake vertices, whose lifetime distribution had an average value of zero and a Gaussian spread determined by the detector resolution, and from secondary vertices originating from charm baryon and B meson decays ('*flying background*' component). The latter component was predicted by the simulation to be $(80 \pm 10)\%$ of the background, both in the right and wrong sign pairs. Its average lifetime was determined from the data using a larger sample of candidate decays reconstructed in the high p_T muon events, as described in [3].

The b-baryon momentum was estimated from the total momentum p_{tot} of the decaying particles using the *residual energy* technique. The residual energy was computed by subtracting the energy associated with the b-baryon candidate (the Λ, the muon and the pion energy) from the total energy associated with charged particles in the hemisphere

containing the Λ and the lepton, defined by the plane perpendicular to p_{tot}. The b-baryon energy was estimated by subtracting this residual energy from the beam energy. The energy associated with all neutral particles in the hemisphere was by definition associated with the b-baryon by this method. The charged pions from the b-baryon decay chain may be wrongly included in the residual energy computation. As discussed in [3], the two effects nearly compensate, the correction factor computed in the simulation to reproduce the generated spectrum being on average 0.97 for unpolarized b-baryons. Sources of systematic error on this factor are the uncertainties on the b-baryon mass and polarization, its momentum spectrum and semi-leptonic decay modes. Their effect on the final lifetime result is listed in table 2. The resolution of the b-baryon momentum predicted by the simulation was 11%, as shown in figure 5. The effect of the non-Gaussian tails of the distribution on the final result of the lifetime fit was found to be negligible (see below).

A maximum likelihood fit was performed simultaneously to the lifetime distribution of the 63 events of the signal sample and to the one of the background vertices described above (300 events) with the likelihood function [3]:

$$L = -\Sigma_i \ln[f(t_i, \sigma_i, \tau, \tau_{bck})],$$

with

$$f(t_i,\sigma_i,\tau,\tau_{bck}) = F_s e^{(\sigma_i^2/2\tau^2 - t_i/\tau)} \cdot \mathrm{erf}\left(\sigma_i/\tau - t_i/\sigma_i)/\sqrt{2}\right)/2\tau + (1-F_s)\cdot \left(F_{fb} e^{(\sigma_i^2/2\tau_{bck}^2 - t_i/\tau_{bck})} \cdot \mathrm{erf}\left(\sigma_i/\tau_{bck} - t_i/\sigma_i)/\sqrt{2}\right)/2\tau_{bck} + F_{nf} e^{-t_i^2/2\sigma_i^2}\right)$$

where τ and τ_{bck} are the signal and background lifetimes; σ_i is the error on the measured decay time t_i; the normalization constant F_s for the signal fraction was fixed to the fitted value of the b-baryon purity discussed above; finally, F_{fb} was the normalization constant for the background fraction from B, D meson decays and $F_{nf} = 1 - F_{fb}$ is the fraction of "non-flying" background. The three parameter fit to the 63 decays in the $\Lambda\mu\nu X$ channel, gave the result:

$$\tau(b\text{-baryon}) = 1.12^{+0.30}_{-0.23}\ \text{ps}$$

with a background lifetime $\tau_{bck} = 1.62^{+0.14}_{-0.10}$ ps and $F_{fb} = 0.79 \pm 0.03$, in agreement with the simulation. The lifetime distributions for the signal events and for the background, together with the probability functions resulting from the fit, are shown in figures 4.c,d. The uncertainties on the magnitude of the flying background and on its lifetime are accounted for in the statistical error of the fit result. The correlation matrix is shown in table 3, where the small anticorrelation between the signal and background lifetimes is quantified. The different contribution to the systematic uncertainty are listed in table 2. The first comes from the uncertainty on the sample composition, while the others affect the estimation of the b-baryon momentum. The assumed value of the average b-baryon mass, M_{bar}, was shifted with respect to the measured mass of the Λ_b, $M(\Lambda_b) = 5640 \pm 50 MeV/c^2$ [1], to take into account the contribution to the observed decay channel of the production of Ξ_b particle (measured to be 5 times smaller than Λ_b production [16]), whose mass is expected to be $250 \pm 50\mathrm{MeV}/c^2$ higher than the Λ_b mass.

The same fitting procedure applied to the Monte Carlo simulation sample gave: $\tau_{bck} = 1.74^{+0.10}_{-0.08}$ ps and $\tau(b\text{-baryon}) = 1.52^{+0.24}_{-0.14}$ ps, compatible with the generated average b-baryon lifetime of 1.56 ps . In the simulation, different samples of b-baryons were generated with average lifetimes varying in the range $0.75 - 2.25$ ps and added in turn

Table 2: Contributions to the systematic error on the average b-baryon lifetime measured using $\Lambda\mu$ correlations.

Error source	variation level	Syst.error(ps)
$b-$baryon purity	0.61 ± 0.07	± 0.04
Λ_c decay mode uncertainty	one st.dev. [12]	± 0.02
$< E_b >$	0.70 ± 0.03	± 0.01
M_{bar}	$5670 \pm 70 MeV$	± 0.015
Λ_b polarization	-0.47 ± 0.47	± 0.01
$\eta(\omega) = \exp[a_{IW}(1-\omega)]$	$a_{IW} = 1.7^{+3.3}_{-1.7}$	± 0.01
$BR(\Lambda_b \to \Lambda_c \ell\nu n\pi)/BR(\Lambda_b \to \Lambda_c \ell\nu)$	$0 \to 0.3$	-0.06
total syst.error	$-$	$^{+0.05}_{-0.08}$

Table 3: Correlation matrix between the variables of the lifetime fit.

$-$	τ	τ_{bck}	F_{fb}
τ	1.00		
τ_{bck}	-0.12	1.00	
F_{fb}	-0.07	-0.18	1.00

to hadronic Z events in which all the other sources of flying background were kept with constant lifetimes. The number of b-baryons in the sample was chosen to reproduce the purity observed in the data. The response of the fitting procedure was linear, without any bias over the whole time interval considered. Summing the systematic uncertainties listed in table 2 in quadrature gives an overall systematic uncertainty of $^{+0.05}_{-0.08}$ ps , much smaller than the statistical uncertainty from the fit.

5 $\Lambda_c \ell$ channel

In this section a study of Λ_b semileptonic decays using fully reconstructed Λ_c is presented, based on the data collected in the 1991 and 1992. Possible sources of Λ_c ($\bar{\Lambda}_c$) ℓ^- (ℓ^+) in the same jet are Λ_b semileptonic decays, B meson semileptonic decays and accidental correlations of a Λ_c and a lepton. The $\Lambda_c \ell$ combinations from Λ_b decays are characterized by higher invariant mass and higher transverse and longitudinal momentum of the lepton than the background pairs from accidental correlations. The contribution of the B meson semileptonic decay to a Λ_c was estimated to be negligible, by an argument similar to that used in section 4.

5.1 Λ_c selection

The Λ_c was reconstructed via the decay $\Lambda_c \to pK\pi$. This is the most abundant decay mode but it is accompanied by a large combinatorial background. In order to enhance the signal, kinematic selection criteria on the Λ_c candidates were optimized using the simulation. The Λ_c was only accepted if the candidate's momentum was greater than 10

GeV/c and if the proton momentum was greater than the π momentum and also greater than 5 GeV/c. The protons and kaons were identified by the RICH or by requiring that their dE/dx measurements be within 2 standard deviations of the expected values. In addition, all three tracks were required to have at least 2 hits in the VD, the χ^2 probability of the 3-prong fitted vertex was required to exceed 0.01 and the flight distance in the $r\phi$ plane, L_T, was required to be greater than $350\mu m$. Figure 6 shows the $pK\pi$ invariant mass distribution obtained. A fit to the $pK\pi$ invariant mass distribution using a Gaussian distribution superimposed on a linear background yields a signal of 137 ± 30 events.

5.2 $\Lambda_c\ell$ correlations

To improve the Λ_c efficiency in events with an identified lepton, the cut described above on the flight distance of the Λ_c candidate was relaxed, requiring only $L_T > 0$. The Λ_c candidates were paired with identified leptons with momenta greater than 3 GeV/c within a cone of 45° around the Λ_c direction. The lepton was required to have a p_T greater than 0.6 GeV/c. The total momentum of the lepton and of the Λ_c was required to be greater than 18 GeV/c and the invariant mass of the Λ_c μ (Λ_c e) pair was required to exceed 3.5 GeV/c^2 (3.3 GeV/c^2). The $M(pK\pi)$ invariant mass spectrum of Λ_c^+ (Λ_c^-) candidates associated with a ℓ^- (ℓ^+) in the same jet is shown in figure 7a. A signal of 29.1 ± 7.5 events (18.5 ± 5.7 $\Lambda_c\mu$ and 10.6 ± 4.4 $\Lambda_c e$ events) around the nominal Λ_c mass is visible. No peak was found in the $pK\pi$ mass distribution for Λ_c candidates with a lepton of the same sign in the same jet (figure 7b).

The signal in figure 7a was interpreted as coming from b-baryon$\rightarrow$ $\Lambda_c l\nu X$ decays. The contribution to the right sign sample from accidental combinations of a Λ_c and a lepton and from Λ_c-lepton pairs from B meson decay was estimated to be negligible. No contribution from the Λ_c signal could be attributed to a kinematical reflection of a D^+ decaying into $K\pi\pi$ or a D_s^+ decaying into $KK\pi$.

The simulation of the decay $\Lambda_b \rightarrow \Lambda_c\mu\nu$ gives an overall efficiency of selection and reconstruction of $(7.2 \pm 0.6)\%$ in the decay mode $\Lambda_c \rightarrow pK\pi$. If one or more pions are produced in the Λ_b semileptonic decays, the efficiency becomes $(3.07 \pm 0.26)\%$ (assuming up to a maximum of 30% of decay modes with 1 or 2 pions, in equal amounts) due to the softer spectrum of the Λ_c and of the μ. This effect was included in the systematic uncertainties.

Using the measured rate $\mathrm{Br}(\Lambda_c \rightarrow pK\pi) = (4.4 \pm 0.6)\%$ [12], this leads to a production rate:

$$f(\mathrm{b}\rightarrow b\text{-baryon}) \times Br(b\text{-baryon}\rightarrow \Lambda_c\mu\nu X) = (1.19 \pm 0.34^{+0.31}_{-0.21})\%.$$

The overall simulated reconstruction efficiency of $(4.6 \pm 0.6)\%$ for the decays $\Lambda_b \rightarrow \Lambda_c e\nu$ gives a production rate:

$$f(\mathrm{b}\rightarrow b\text{-baryon}) \times Br(b\text{-baryon}\rightarrow \Lambda_c e\nu X) = (1.15 \pm 0.44^{+0.31}_{-0.21})\%.$$

Assuming lepton universality:

$$f(\mathrm{b}\rightarrow b\text{-baryon}) \times Br(b\text{-baryon}\rightarrow \Lambda_c \ell\nu X) = (1.18 \pm 0.26^{+0.31}_{-0.21})\%.$$

Table 4 summarizes the different contributions to the systematic error.

Table 4: Contributions to the total systematic uncertainty on the b-baryon production rate times the branching ratio to $\Lambda_c \ell \nu X$.

source of uncertainty	variation level	Syst.uncertainty($\times 10^2$)
Λ_b sel. + rec. efficiency	$(7.2 \pm 0.6)\%$	± 0.09
Λ_c branching fraction	$(4.4 \pm 0.6)\%$	± 0.15
Λ_b polarization	-0.47 ± 0.47	± 0.09
$\eta(\omega) = \exp[a_{IW}(1-\omega)]$	$a_{IW} = 1.7^{+3.3}_{-1.7}$	± 0.06
$\mathrm{Br}(\Lambda_b \to \Lambda_c \ell \nu \mathrm{n}\pi)/\mathrm{Br}(\Lambda_b \to \Lambda_c \ell \nu)$	$0 \to 0.3$	$+0.23$
total syst.uncertainty	–	$^{+0.31}_{-0.21}$

5.3 Measurement of b-baryon lifetime

In the $\Lambda_c \ell \nu X$ channel, b-baryon candidate vertices were reconstructed using the trajectories of the Λ_c and the lepton to fit a common vertex. The Λ_b momentum was estimated with the missing energy technique:

$$E_{\Lambda_b} = E_{beam} - E_{visible} + E_{\Lambda_c} + E_\ell$$

where $E_{visible}$ was the sum of the energies of both charged and neutral particles in the same hemisphere as the Λ_c. The quantity $E_{beam} - E_{visible}$ measured the neutrino energy in the b-baryon semileptonic decay (this was not true in the $\Lambda\ell$ analysis, where the Λ_c decay was not fully reconstructed), provided that only the 3-body $\Lambda_c \ell \nu$ decay mode was present. In this case, the simulation showed that the momentum used must be scaled by the factor 0.950 ± 0.015, where the uncertainty was due to the finite statistics available.

If one or two additional pions were produced in the Λ_b decay, the estimator gave a Λ_b energy that was on average respectively 3.5 or 6 GeV too low, but this effect was reduced by the lower efficiency of the many-π modes with respect to the 0-π mode.

A sample of 28 signal vertices was selected using right sign $\Lambda_c \ell$ pairs with $2.260 < M(pK\pi) < 2.310$ GeV/c^2. The b-baryon purity of this sample was determined from a fit to the data to be $(60 \pm 20)\%$. In a similar way, a sample of 139 background vertices was selected with wrong sign pairs with $2.085 < M(pK\pi) < 2.485$ GeV/c^2 and sideband right sign pairs ($2.085 < M(pK\pi) < 2.240$ GeV/c^2 and $2.330 < M(pK\pi) < 2.485$ GeV/c^2).

The reconstructed Λ_c track and the lepton were fitted to a common secondary vertex (the b-baryon candidate decay vertex); the proper time distributions of the signal and background samples, shown in figure 7c and 7.d respectively, were fitted with the same technique used for the study of the $\Lambda\ell$ channel. The result is:

$$\tau(b\text{-baryon}) = 1.33^{+0.71+0.08}_{-0.42-0.09} \text{ ps } (\Lambda_c \ell \nu X \text{ channel, 28 decays}).$$

with a flying background lifetime of $1.52^{+0.28}_{-0.21}$ ps; the correlation matrix of the fit parameters is shown in table 5. The fitted flying background fraction was 0.63 ± 0.05. The different contributions to the systematic error are shown in table 6. The effects of the Λ_b polarization have been studied with the simulation and found to be negligible.

6 Muon-proton channel

In the analysis of this channel, semileptonic decays of b-baryons were selected by the presence of a muon and a proton of high momenta and opposite charges in the same jet. About 500,000 hadronic events recorded in 1992 with the barrel gas RICH operational

Table 5: Correlation matrix between the variables of the lifetime fit in the $\Lambda_c\ell$ sample.

	τ	$\tau_{\rm bck}$	$F_{\rm fb}$
τ	1.00		
$\tau_{\rm bck}$	-0.14	1.00	
$F_{\rm fb}$	-0.04	-0.27	1.00

Table 6: Contributions to the systematic error on the average b-baryon lifetime measured using $\Lambda_c\ell$ correlations.

Error source	variation level	Syst.error(ps)
$b-$baryon purity	0.60 ± 0.20	± 0.08
Monte Carlo statistics	–	± 0.02
$M_{\rm bar}$	$5670 \pm 70 MeV$	± 0.015
$Br(\Lambda_b \to \Lambda_c \ell\nu n\pi)/Br(\Lambda_b \to \Lambda_c \ell\nu)$	$0 \to 0.3$	-0.04
total syst.error	–	$^{+0.08}_{-0.09}$

were used. Proton selection used the measurement of the specific energy loss in the TPC (dE/dx) and the detection of Cherenkov photons in the RICH. The proton is thought to come predominantly from the chain decay b-baryon $\to \mu\bar{\nu}_\mu c$-baryon, c-baryon $\to$ pX. It is noted that the flight distance of the secondary charm baryon is, on average, much less than that of its parent, and that the fast proton follows its direction. To allow for a precise determination of the b-baryon decay vertex, which is essential for the present analysis, the proton and muon candidates were required to have at least two associated hits in the Vertex Detector. Detailed simulations showed that 70% of $\Lambda_b \to \mu\bar{\nu}_\mu$pX decays gave rise to a reconstructed three-dimensional μ-p vertex. These vertices were distributed around the simulated Λ_b decay vertex with a precision of $\pm 300\ \mu m$ in the $r\phi$ plane. The requirement of the detection of the proton in the VD and secondary muon-proton vertex reconstruction substantially reduced backgrounds due to tertiary protons: only (16 ± 7)% of the signal was estimated to be protons from non-charmed hyperon decays in the b-baryon decay chain. This results in an overlap smaller than 5% between this sample and the $\Lambda\mu$ sample discussed above.

6.1 Signal and background characteristics

The signal muon-proton pairs have the following properties: the muon has hard momentum (p_μ) and transverse momentum (p_T) spectra, the proton has a hard momentum ($p_{\rm p}$) spectrum, the muon and proton form a secondary vertex and they have opposite charge. The background is due to genuine protons which do not come from from b-baryon decays and to pions and kaons misidentified as protons, as well as charged hadrons faking muons.

The background involving genuine protons was almost completely eliminated by requiring the proton momentum to be above 8.5 GeV/c and the muon momentum above 4 GeV/c. The background involving fake protons is dominated by charged kaons. At low p_T the muon-kaon pairs are predominantly of opposite charge whereas at high p_T the background is mostly same sign pairs. This flip in the charge correlation of the background involving kaons is caused by semileptonic b-hadron decays $b \to c\mu^-\bar{\nu}_\mu$ followed by

a $c \to sX$ transition dominating at high p_T and semileptonic decays of primary and secondary charm hadrons $c \to s\mu^+\nu_\mu$ dominating at low p_T. Because of this, the procedure of removing events below a given transverse momentum of the muon and subtracting the wrong charge correlation, used in the analyses of $\Lambda\ell$ and $\Lambda_c\ell$ channels, was not followed.

Instead, a global fit (see section 6.3) to the muon p_T spectrum, the hadron dE/dx distribution and the proper time distribution of reconstructed muon-hadron vertices was applied to the separate samples of muon-hadron pairs enriched in protons, kaons and pions simultaneously. These samples were obtained with the use of the RICH as explained in the next section. In this way the yield of b-baryon signal and its average lifetime was extracted using all charged hadron identification information and minimizing the dependence on the simulation.

6.2 Sample Definition

6.2.1 Hadron Identification

Hadrons[†] were selected in a momentum range where energetic kaons and protons could be separated by the gas radiator of the RICH, namely $p \geq 8.5$ GeV/c. In this range, the expected mean number of Cherenkov photons detected for a kaon by the RICH was greater than 1.5. Protons up to 16 GeV/c are below the Cherenkov threshold. K/p separation was effective up to 30 GeV/c and covered most of the high momentum part of the spectrum of the signal protons.

Using the information provided by the RICH, four separate samples of energetic charged hadrons were defined:

- the proton sample. This contained tracks whose proton hypothesis probability exceeded 90%. This cut suppressed kaons and pions sufficiently to make the p:K:π ratio approximately 1:1:1.
- the kaon sample. This contained tracks whose kaon hypothesis probability exceeded 80%. This cut removed all protons and gave a K/π ratio greater than 2.
- the pion sample. This required that the pion hypothesis probability exceeded 25% and that more than 5 Cherenkov photons were compatible with the pion hypothesis. All protons and kaons in this data set were suppressed by this cut.
- the unresolved hadron sample taking all tracks not accepted in the previous three samples.

The composition of these samples was determined using dE/dx measurement from the TPC. In the momentum range above 8.5 GeV/c pions, kaons and protons are on the relativistic rise of the dE/dx. The mean values of their energy loss differ by approximately constant amounts from ~ 4 GeV/c up to ~ 25 GeV/c. Requiring at least 30 hit TPC wires to analyse a track, the ratios $\frac{dE}{dx}/T_j(p)$ of the measured mean energy loss to the momentum dependent theoretical values $T_j(p)$ (j = p,K,π) have Gaussian distributions with a common precision of $\pm 7\%$. The consistency between the theoretical and observed specific ionization was checked on the four samples described above. This ensured a very good parameterization of the specific ionization measurement, independent of the simulation.

6.2.2 Muon-Hadron Selection

The selection procedure consisted of three sets of cuts, which will be referred to in the determination of the selection efficiency (section 6.4):

[†] In what follows *hadron* stands for a charged particle not identified as a muon.

1. Event and muon selection: In addition to the hadronic event selection described in section 3 a successfully reconstructed primary vertex was required, formed by at least three charged tracks with the χ^2 probability of the vertex fit greater then 1%. The muon candidate selection (section 3.2) was complemented by the requirement that the muon candidate had at least two associated hits in the Vertex Detector and a momentum above 4 GeV/c. These cuts defined the event sample used for the determination of the number of muons from b decay (see section 6.4) and to which the muon-hadron vertex search was applied.
2. Hadron track quality cuts: hadrons were accepted when the information from the RICH was available for the hadron track, when the hadron track had at least two associated hits in the Vertex Detector, and more than 30 wires used for the dE/dx measurement.
3. Muon-hadron vertex definition: muon-hadron pairs were accepted when the hadron had a momentum above 8.5 GeV/c, when the muon and the hadron were in the same jet, when the muon-hadron secondary vertex had a probability greater than 1%, and the error on the distance δ_V between the primary and the secondary vertices was smaller than 1mm.

Combining these three sets of cuts with the RICH selection described in the previous section, four samples of muon-hadron pairs were obtained: the muon-proton sample (μp) and the muon-kaon (μK), muon-pion ($\mu\pi$) and muon-unresolved (μX) control samples[‡].

6.3 b-baryon Lifetime

6.3.1 Global Fit Procedure

A maximum likelihood fit was used to estimate the number of muon-proton pairs from b-baryon decays and the average lifetime of b-baryons.

For each μ-hadron event, the dE/dx, the signed muon transverse momentum $p_T^{(S)} = S \cdot p_T$ (where $S = +1$ for the *right sign* and $S = -1$ for the *wrong sign* correlation), and $t = \delta_V/(p_{bar}/M_{bar})$, where δ_V is the distance of the μ-hadron vertex from the primary vertex, were considered as a set of three independent measurements. The last quantity estimated the b-baryon proper time assuming the event belongs to the signal. To compute it, the b-baryon momentum p_{bar} was evaluated using a linear relationship with respect to $|\vec{p_\mu} + \vec{p_{\rm p}}|$ obtained in the simulation ($\sim \pm 16\%$ accuracy at 13 GeV/c and $\sim \pm 6\%$ at 35 GeV/c).

Six classes of events were distinguished: (1) the signal, the backgrounds involving (2) protons, (3) kaons from b-hadron decays, (4) other kaons, (5) pions from b-hadron decays and (6) other pions.

Each class had its own probability density function (*pdf*) being the product of the three *pdf*'s associated to each of the measured quantities:

$$\mathcal{P}(p_T^{(S)}, \tfrac{dE}{dx}, t|class) = \mathcal{P}_\perp(p_T^{(S)}|class) \cdot \mathcal{P}_{\frac{dE}{dx}}(\tfrac{dE}{dx}, \sigma_{\frac{dE}{dx}}|class) \cdot \mathcal{P}_t(t, \sigma_t|class)$$

The $\mathcal{P}_\perp$ probability density functions were taken from the simulation. In this *pdf* the distinction between different 'kaon' classes (3 and 4) and 'pion' classes (5 and 6) were preserved to allow for variations in the muon transverse momentum distributions resulting from the two components of the backgrounds of kaons and pions.

[‡]In the following, the notation μi will be used to refer generically to one of these four samples.

The $\mathcal{P}_{\frac{dE}{dx}}$ probability density function was taken to be:

$$\mathcal{P}_{\frac{dE}{dx}}(\tfrac{dE}{dx}, \sigma_{\frac{dE}{dx}}|j) = \frac{1}{\sqrt{2\pi}\sigma_{\frac{dE}{dx}}} \exp\left(-\frac{(\frac{dE}{dx}/T_j - 1)^2}{2\sigma_{\frac{dE}{dx}}{}^2}\right)$$

where T_j were momentum dependent theoretical mean values of the dE/dx for the hadron from the class j.

The signal $\mathcal{P}_t$ probability density function was parameterized as a convolution of an exponential decay probability density function of mean $\tau_{\mu\mathrm{p}}$ and a Gaussian resolution function. The kaon and pion background $\mathcal{P}_t$ probability density functions were taken as linear combinations of a flying part (fraction $f_{\mathrm{BGD}}(\mathrm{K\ or}\ \pi)$ described by a convolution of an exponential decay of effective lifetime $\tau_{\mathrm{BGD}}(\mathrm{K\ or}\ \pi)$, and a resolution function) and a 'non flying' part (fraction 1-f_{BGD} described by a resolution function alone). These four parameters, $\tau_{\mathrm{BGD}}(\mathrm{K})$, $\tau_{\mathrm{BGD}}(\pi)$, $f_{\mathrm{BGD}}(\mathrm{K})$ and $f_{\mathrm{BGD}}(\pi)$, were determined by the fit. For the $\mathcal{P}_t$ probability density function of the proton background two extreme parameterizations were used: the pion one and a Gaussian parameterization. The final results were obtained by averaging the results of the fits performed with these two parameterizations of the proton background $\mathcal{P}_t$ *pdf*, taking half of the difference as a contribution to the systematic error.

The following negative log-likelihood function was minimized by the fit:

$$L = -\sum_{\mu i}\sum_{n=1}^{N_{\mu i}} \ln\left(\sum_{class=1}^{6} \mathcal{F}(class|\mu i)\mathcal{P}([p_T^{(S)}, \tfrac{dE}{dx}, t]_n|class)\ ,\right)$$

where $N_{\mu i}$ was the population of sample μi and $\mathcal{F}(class|\mu i)$ was the fraction of events in sample μi coming from the given class. The 24 composition parameters $\mathcal{F}(class|\mu i)$ were constrained by four normalization conditions (one for each sample): $\sum_{j=1}^{6}\mathcal{F}(j|\mu i) = 1$. Moreover, the relative contents $\mathcal{F}(j|\mu i)/\mathcal{F}(j+1|\mu i)$ of the proton classes ($j = 1$), the kaon classes ($j = 3$) and the pion classes ($j = 5$) were the same in each sample. This left 11 independent fractions to be determined by the fit. The proton content in the three control samples and the kaon content in the $\mu\pi$ sample were found by the fit to be compatible with zero and were fixed to zero in the final fit, leaving only seven composition parameters to be determined. The systematic effect introduced by this assumption was taken into account in the contributions from the background composition.

6.3.2 Results of the Fit

The fit was performed with 125 events of the μp sample, 243 events of the μK sample, 295 events of the $\mu\pi$ sample and 369 events of the μX sample.

The projections of the fit space onto the $p_T^{(S)}$, $\zeta = (\frac{dE}{dx}/T_{\mathrm{p}} - 1)/\sigma_{\frac{dE}{dx}}$ and t axes are shown in figures 8, 9, and 10 respectively. The purity of the signal can be read from figure 11 where additional cuts on $p_T^{(S)} > 0.7\mathrm{GeV}/c$ and $\zeta < 1.5$ were applied to the μp sample. The number of signal events present in the muon-proton sample was estimated to be $N(\mu\mathrm{p\ from}\ b\text{-baryon}) = 28.9^{+6.7}_{-6.2}\ ^{+1.8+0.9}_{-2.6-0.4}$. The average lifetime of b-baryons was estimated to be

$$\tau_{\mu\mathrm{p}} = \left\{1.27^{+0.35}_{-0.29} \pm 0.09(syst.exp.) \pm 0.02(syst.theory)\right\}\mathrm{ps}\ .$$

The first systematic error was due to the measurement procedure, whereas the second represents the influence of unknown b-baryon properties.

The estimates of the seven composition variables chosen as fit parameters, together with the five variables involved in the lifetime part of the likelihood function are reported in table 7.

The correlation matrix for the variable parameters is given in table 8. The "composition" parameters ($P_1 - P_7$) and the "lifetime" parameters ($P_8 - P_{12}$) are practically uncorrelated. There was no parameter correlated to the mean b-baryon lifetime (P_8) by more than $\sim$12%.

Table 7: The result of the maximum likelihood fit of the average b-baryon lifetime and the composition of the selected samples. The first error quoted comes from the fit, the second is half the difference between the results corresponding to the two different proton background parameterizations.

Parameter	Result
P_1: fraction of signal in the μp sample	$0.233 \pm ^{0.054}_{0.050} \pm 0.002$
P_2: ratio (signal)/(all p)	$0.75 \pm 0.15 \pm 0.02$
P_3: ratio (K from b)/(all K)	$0.557 \pm ^{0.053}_{0.051} \pm 0.001$
P_4: ratio (π from b)/(all π)	$0.453 \pm ^{0.057}_{0.056} \pm 0.001$
P_5: fraction of kaons in the μp sample	$0.354 \pm ^{0.105}_{0.095} \pm 0.009$
P_6: fraction of kaons in the μK sample	$0.858 \pm ^{0.039}_{0.038} \pm 0.001$
P_7: fraction of kaons in the μX sample	$0.467 \pm ^{0.044}_{0.042} \pm 0.001$
P_8: average lifetime of b-baryon $\tau_{\mu p}$	$1.27 \pm ^{0.35}_{0.29} \pm 0.03$ ps
P_9: $\tau_{\rm BGD}$(K)	$1.51 \pm ^{0.29}_{0.25} \pm 0.002$ ps
P_{10}: $\tau_{\rm BGD}(\pi)$	$1.84 \pm ^{0.19}_{0.17} \pm 0.001$ ps
P_{11}: $f_{\rm BGD}$(K)	$0.64 \pm 0.09 \pm 0.001$
P_{12}: $f_{\rm BGD}(\pi)$	$0.731 \pm ^{0.047}_{0.050} \pm 0.000$

6.3.3 Fit Systematics

The parameters P_3 and P_4 describe the relative amount of true kaons and pions arising from b-hadron decays among all kaons and pions. To examine relevant systematic effects, three approaches were taken: (1) three different definitions of these parameters were used (a) $\frac{\text{K }(\pi)\text{ from b}}{\text{all K }(\pi)}$, (b) $\frac{\text{K }(\pi)\text{ and }\mu\text{ from b}}{\text{all K }(\pi)}$, (c) $\frac{\text{K }(\pi)\text{ and direct }\mu\text{ from b}}{\text{all K }(\pi)}$; (2) these fractions were fixed to the Monte-Carlo prediction; (3) μK or μX samples were excluded from the fit. The maximal variation of the fit results was taken as a contribution ("K, π bkg composition" in table 9).

To evaluate possible systematics related to the parameterization of the $\mathcal{P}_\perp$ probability density function of the proton background class, this class was divided into four groups characterized by very different $p_T^{(S)}$ spectra of the accompanying muon: (1a) *right sign* muons from b-hadron decays, (1b) *wrong sign* muons from b-hadron decays, (2a) other *right sign* muon candidates (2b) other *wrong sign* muon candidates. From the set of these four groups, 14 non-trivial subsets can be chosen (4 containing one group, 6 containing two groups and 4 containing three groups). The fit was performed 14 times with the $\mathcal{P}_\perp$ probability density function of the proton background sample determined after the chosen subset was scaled up by a factor of 2. The maximal variation was taken as an estimate of the systematic effects ("p bkg composition" in table 9).

The results quoted were obtained with p_T calculated including the muon candidate in the jet. To evaluate systematic errors, p_T was replaced (1) by ${p_T}^{out}$ calculated excluding

Table 8: Correlation matrix for the fit parameters. The definitions of the parameters are given in table 7.

P_1	P_2	P_3	P_4	P_5	P_6	P_7	P_8	P_9	P_{10}	P_{11}	P_{12}
.40											
.06	.05										
-.04	-.01	-.03									
-.19	.62	.00	.03								
-.01	-.01	-.11	.08	.00							
-.01	-.01	-.13	.07	.00	.02						
-.01	.09	.00	.01	.09	-.00	-.01					
.02	-.01	-.01	-.01	-.00	.01	.03	-.12				
.01	.01	-.00	-.01	.02	.00	.01	-.02	-.12			
-.05	-.03	-.02	-.02	.04	-.00	.05	-.04	-.22	0.05		
-.01	.01	.00	.01	.00	.02	-.01	-.00	.02	-.20	-.22	

the muon candidate from the jet and (2) by the quadratic sum $\sqrt{(p_T{}^2 + (p_\mu/10)^2)}$. All three definitions were tested with several binnings. The maximal variation was taken as a contribution to the systematic error ("p_T binning/definition" in table 9).

In the likelihood function, the $\mathcal{P}_t$ probability density function was used only for the *right sign* muon-proton sample, and optionally for the part above some p_T cut. Outside this sample $\mathcal{P}_t$ pdf's were fixed to a constant value for all classes. The result was found to be stable within 2% in the range of p_T cut from 0 GeV/c (no cut) to 0.7 GeV/$c$as can be seen in the figure 12. For higher cut values, the b-baryon lifetime begins to fluctuate within increasing statistical error.

The fit procedure was tested in the following way. From the available statistics of signal muon-proton pairs in simulated b-baryon decays passing all the selection cuts, different sets of 28 pairs each were randomly chosen; from each of them a larger test sample of muon-hadron pairs was formed by adding a number of muon-unresolved hadron pairs randomly chosen from real data, in such a way as to reproduce in the test sample the signal fraction 0.23 observed in the data. The generated lifetime of the b-baryon in the simulation was 1.3 ps. The whole fit was repeated several times with the data muon-proton sample replaced by one of the test samples described above. The distributions of the fit result for the proton signal fraction P_1 and for the average b-baryon lifetime P_8 are shown in figures 13a,b respectively; their average values reproduced the known input values of the parameters, with a spread in agreement with the average fit error.

6.4 Branching Ratio

The number of signal events found by the fit was used for the calculation of the following production rate:

$$f(\mathrm{b} \to b\text{-baryon}) \times \mathrm{BR}(b\text{-baryon} \to \mathrm{p}\mu\bar{\nu}_\mu\mathrm{X}) = (0.49 \pm 0.11 \pm 0.06^{+0.14}_{-0.09})\%.$$

The first systematic error is due to the measurement procedure, whereas the second represents the influence of unknown b-baryon properties. Systematic effects are sumarized in table 10. The total experimental systematic error results from the following sources listed in the table:

- $N(\mu\mathrm{p}$ from b-baryon) is the number of signal events found in the previous section.

Table 9: Systematic uncertainties in the fit.

source of variation	variation level	resulting variation of	
		$N(\mu\mathrm{p}$ from b-baryon) [events]	$\tau_{\mu\mathrm{p}}$ [ps]
Experimental systematics			
dE/dx normalization	one stand. dev.	± 1.2	± 0.03
p_T binning/definition	see text	$^{+1.2}_{-2.3}$	± 0.08
K, π bkg composition	see text	± 0.2	± 0.01
p bkg composition	see text	$^{+0.6}_{-0.3}$	± 0.01
p background $\mathcal{P}_t$ *pdf*	see text	± 0.3	± 0.03
boost estimate	one stand. dev.	—	± 0.03
total systematic error (measurement)		$^{+1.8}_{-2.6}$	± 0.09
Systematic uncertainty due to unknown b-baryon properties			
b-baryon polarization	-0.47 ± 0.47	± 0.3	± 0.01
$\Lambda_\mathrm{b} \to \Lambda_\mathrm{c} \mu \bar{\nu}_\mu$ decay form factor			
$\eta(\omega) = \exp[a_{IW}(1-\omega)]$	$a_{IW} = 1.7^{+3.3}_{-1.7}$	± 0.1	± 0.01
$\langle E(b\text{-baryon})\rangle / E(\mathrm{beam})$	0.70 ± 0.03	± 0.1	± 0.01
$\mathrm{BR}(\Lambda_\mathrm{b} \to \Lambda_\mathrm{c} \ell \bar{\nu})/\mathrm{BR}(\Lambda_\mathrm{b} \to \ell \bar{\nu} \mathrm{X})$	$1.0 \to 0.7$	$+0.9$	$+0.02$
total systematic uncertainty (theory)		$^{+0.9}_{-0.4}$	± 0.02

Table 10: Contributions to the total systematic uncertainty of the b-baryon production rate times its branching ratio into pμX. (For definitions of the efficiencies ϵ_1, ϵ_2, ϵ_3, ϵ_R and the correction C_Λ see text.)

quantity	value	contribution $\times 10^2$
Experimental systematics		
$N(\mu\mathrm{p}$ from b-baryon)	$28.9\ ^{+1.8}_{-2.6}$(syst.)	$^{+0.03}_{-0.04}$
ϵ_1	$0.376\ \pm 0.011$	± 0.02
ϵ_2	$0.308\ \pm 0.009$	± 0.02
ϵ_3	$0.195\ \pm 0.012$	± 0.03
ϵ_R	$1.0\ -0.06$	$+0.03$
Total Systematic Uncertainty (measurement)		± 0.06
Systematic uncertainty due to unknown b-baryon properties		
C_Λ	$0.84\ \pm 0.07$	± 0.04
b-baryon polarization	$-0.47\ \pm 0.47$	± 0.07
$\Lambda_\mathrm{b} \to \Lambda_\mathrm{c} \mu \bar{\nu}_\mu$ decay form factor		
$\eta(\omega) = \exp[a_{IW}(1-\omega)]$	$a_{IW} = 1.7\ ^{+3.3}_{-1.7}$	$^{+0.09}_{-0.03}$
$\langle E(b\text{-baryon})\rangle / E(\mathrm{beam})$	$0.70\ \pm 0.03$	± 0.03
$\mathrm{BR}(\Lambda_\mathrm{b} \to \Lambda_\mathrm{c} \ell \bar{\nu})/\mathrm{BR}(\Lambda_\mathrm{b} \to \ell \bar{\nu} \mathrm{X})$	$1.0 \to 0.7$	$+0.06$
Total Systematic uncertainty (theory)		$^{+0.14}_{-0.09}$

- ϵ_1 is the efficiency of the "event and muon" selection (the first item in the Section 6.2.2).
- ϵ_2 is the efficiency of the hadron track quality cuts (the second item in the Section 6.2.2). This efficiency was found in the data.
- ϵ_3 is the efficiency of the additional selection defined in the third item of the Section 6.2.2. This efficiency was found using simulation.
- ϵ_R is the efficiency of the selection of the μp sample with the RICH. This efficiency was found by the fit (before fixing to zero proton contents in the control samples).

Entries for the theoretical systematics are similar to those described in the analysis of the $\Lambda\ell$ channel. C_Λ is the correction due to the residual presence of protons from the chain decay b-baryon$\rightarrow$ c-baryon$\rightarrow$hyperon$\rightarrow$proton.

7 Conclusions

The production and lifetime of the b-baryon has been studied with three different and complementary methods, relying on the detection of a fast Λ, a Λ_c and a fast proton in the same jet as a high p_T lepton. The following semi-exclusive branching ratios have been measured:

$$f(\mathrm{b} \rightarrow b\text{-baryon}) \times \mathrm{BR}(b\text{-baryon} \rightarrow \Lambda\ell\bar{\nu}_\ell \mathrm{X}) = (0.30 \pm 0.06 \pm 0.04)\%,$$
$$f(\mathrm{b} \rightarrow b\text{-baryon}) \times \mathrm{BR}(b\text{-baryon} \rightarrow \Lambda_c\ell\bar{\nu}_\ell \mathrm{X}) = (1.18 \pm 0.26^{+0.31}_{-0.21})\%,$$
$$f(\mathrm{b} \rightarrow b\text{-baryon}) \times \mathrm{BR}(b\text{-baryon} \rightarrow \mathrm{p}\mu\bar{\nu}_\mu \mathrm{X}) = (0.49 \pm 0.11^{+0.15}_{-0.11})\%.$$

From partially reconstructed b-baryon decay candidates in these three different semi-leptonic channels, the following values for the average b-baryon lifetime have been measured:

$$\tau(b\text{-baryon}) = 1.12^{+0.30+0.05}_{-0.23-0.08} \text{ ps (63 decays, } \Lambda\mu\bar{\nu}_\mu \mathrm{X} \text{ channel)},$$
$$\tau(b\text{-baryon}) = 1.33^{+0.71+0.08}_{-0.42-0.09} \text{ ps (28 decays, } \Lambda_c\ell\bar{\nu}_\mu \mathrm{X} \text{ channel)},$$
$$\tau(b\text{-baryon}) = 1.27^{+0.35}_{-0.29} \pm 0.09 \text{ ps (47 decays, } \mathrm{p}\mu\bar{\nu}_\mu \mathrm{X} \text{ channel)}.$$

The above lifetime determinations rely on completely independent event samples. This was checked on an event by event basis for the μ-proton and μ-Λ_c samples, where a small overlap could not be excluded a priori by the selection criteria discussed above. The overlap between the $\mu - \Lambda$ and the μ-proton samples was found negligible by the simulation, as discussed in section 6. The common systematics, due to the modelling of the b-baryon production and decay properties, can be inferred from tables 2, 6 and 7.

Averaging the three results, under the assumption that the different b-baryon species enter in the same proportion in the decay channels considered (all of them are expected in fact to be largely dominated by the Λ_b baryon), gives the mean b-baryon lifetime:

$$\tau(b\text{-baryon}) = 1.21^{+0.21}_{-0.18} \pm 0.04(exp.syst.)^{+.02}_{-.07}(th.syst.) \text{ ps}.$$

Acknowledgements

We are greatly indebted to our technical collaborators and to the funding agencies for their support in building and operating the DELPHI detector, and to the members of the CERN-SL Division for the excellent performance of the LEP collider.

References

[1] UA1 Collaboration, C. Albajar *et al.*, Phys. Lett. **B273** (1992) 540.

[2] ALEPH Collaboration, D. Decamp *et al.*, Phys. Lett. **B278** (1992) 209.
OPAL Collaboration, P. D. Acton *et al.*, Phys. Lett. **B281** (1992) 394.

[3] DELPHI Collaboration, P. Abreu *et al.*, Phys. Lett. **B311** (1993) 379.

[4] ALEPH Collaboration, D. Buskulic *et al.*, Phys. Lett. **B297** (1992) 449;
OPAL Collaboration, R. Akers *et al.*, Phys. Lett. **B316** (1993) 435.

[5] I.I. Bigi and N.G. Uraltsev, Phys. Lett. **B280** (1992) 271;
G. Altarelli and S. Petrarca, Phys. Lett. **B261** (1991) 303.

[6] DELPHI Collaboration, P. Aarnio *et al.*, Nucl. Instr. Meth. **A303** (1991) 233.

[7] E.G. Anassontzis *et al.*, Nucl. Instr. Meth. **A323** (1992) 351.

[8] DELPHI Collaboration, P. Abreu *et al.*, Nucl. Phys. **B418** (1994) 403.

[9] C. Kreuter, Ph.D Thesis, Karlsruhe University, IEKP-KA/93-9.

[10] W. Adam *et al.*, "Analysis techniques for the DELPHI RICH", Contributed paper GLS0188, to the 27th International Conference on High Energy Physics, Glasgow 1994.

[11] T. Sjostrand et al., Comput.Phys.Commun. **39** (1986) 346; **43** (1987) 347.

[12] The Particle Data Group, Phys. Rev. **D50** (1994) 1173.

[13] CLEO Collab., G. Crawford *et al.*, Phys. Rev. **D45** (1992) 752.

[14] T. Sjöstrand, Comp. Phys. Comm. **82** (1994) 74.

[15] N. Isgur and M.B. Wise, Phys. Lett. **B232** (1989), 113;
N. Isgur and M.B. Wise, Phys. Lett. **B237** (1990), 527.

[16] DELPHI Collaboration, "Production of strange B-baryons decaying into $\Xi^{\mp}\ -\ \ell^{\mp}$ pairs at LEP", CERN-PPE/95–29, to be published in Zeit. f. Phys. C.

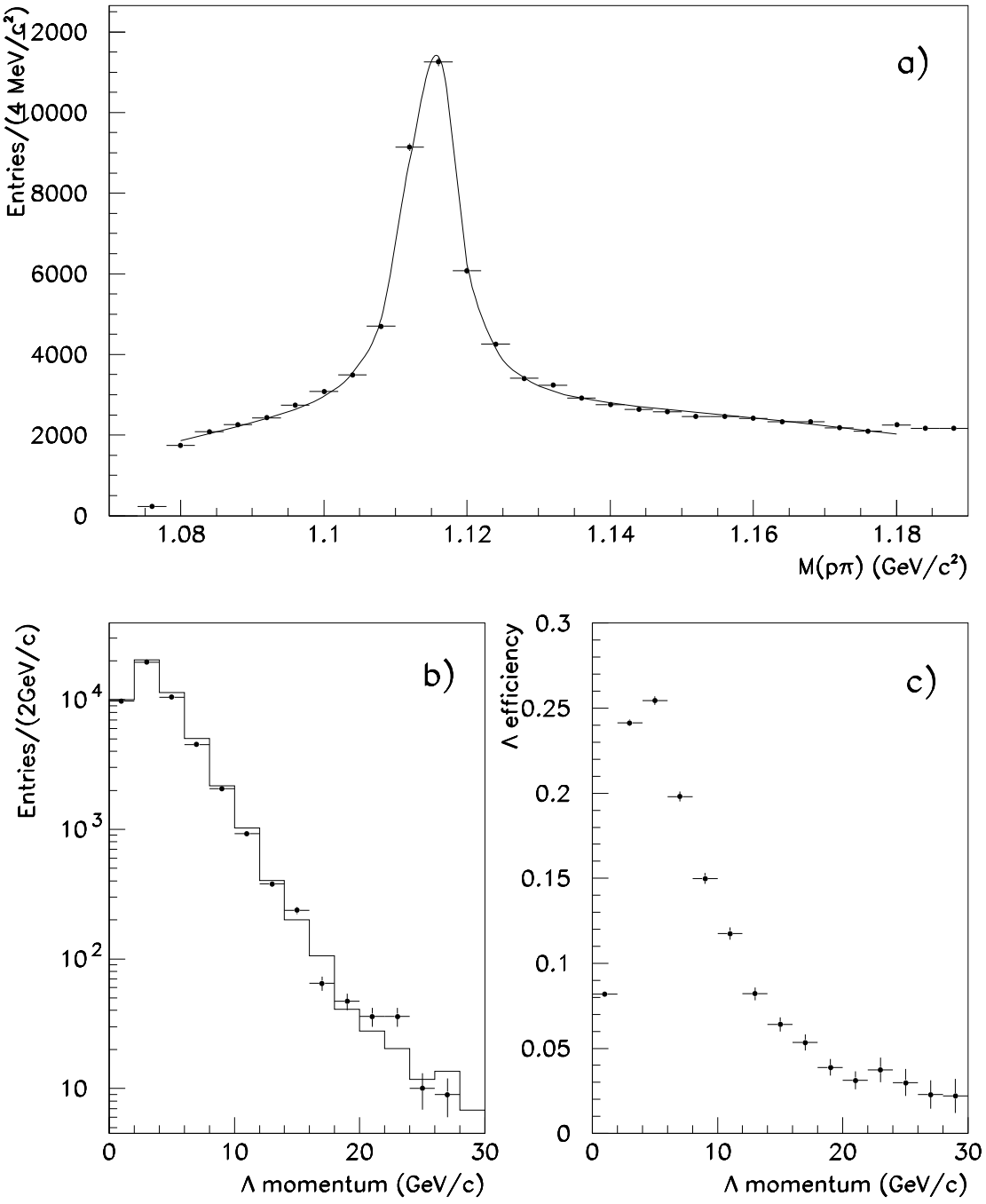

Figure 1: a) $p\pi^-$ invariant mass distribution for Λ candidates with $p > 4GeV/c$; the curve is the result of a fit using a Breit-Wigner function, which takes into account the variation of the mass resolution with the momentum of the decaying tracks, and a polynomial background. b) Background subtracted Λ momentum spectrum (dots: data; histogram: Monte Carlo simulation) ; c) $\Lambda \to p\pi^-$ reconstruction efficiency computed in the simulation.

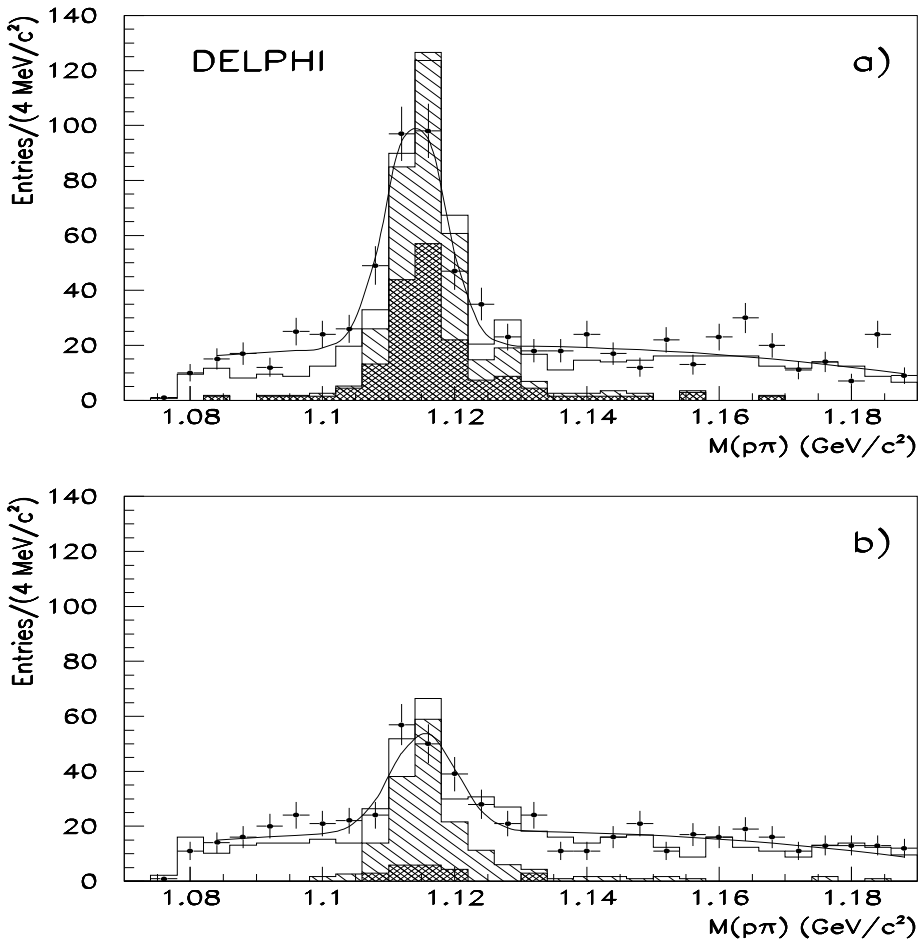

Figure 2: Distribution of pπ invariant mass for Λ candidates correlated to high p_T leptons in the same jet: a) right-sign pairs; b) wrong-sign pairs. The data are shown by the points; the simulation, normalised to the total number of hadronic Z decays, as a histogram: the contribution from b-baryon decay is shown double-hatched, while the background from fragmentation Λ's is shown single-hatched. The curves show the result of the fit described in the text.

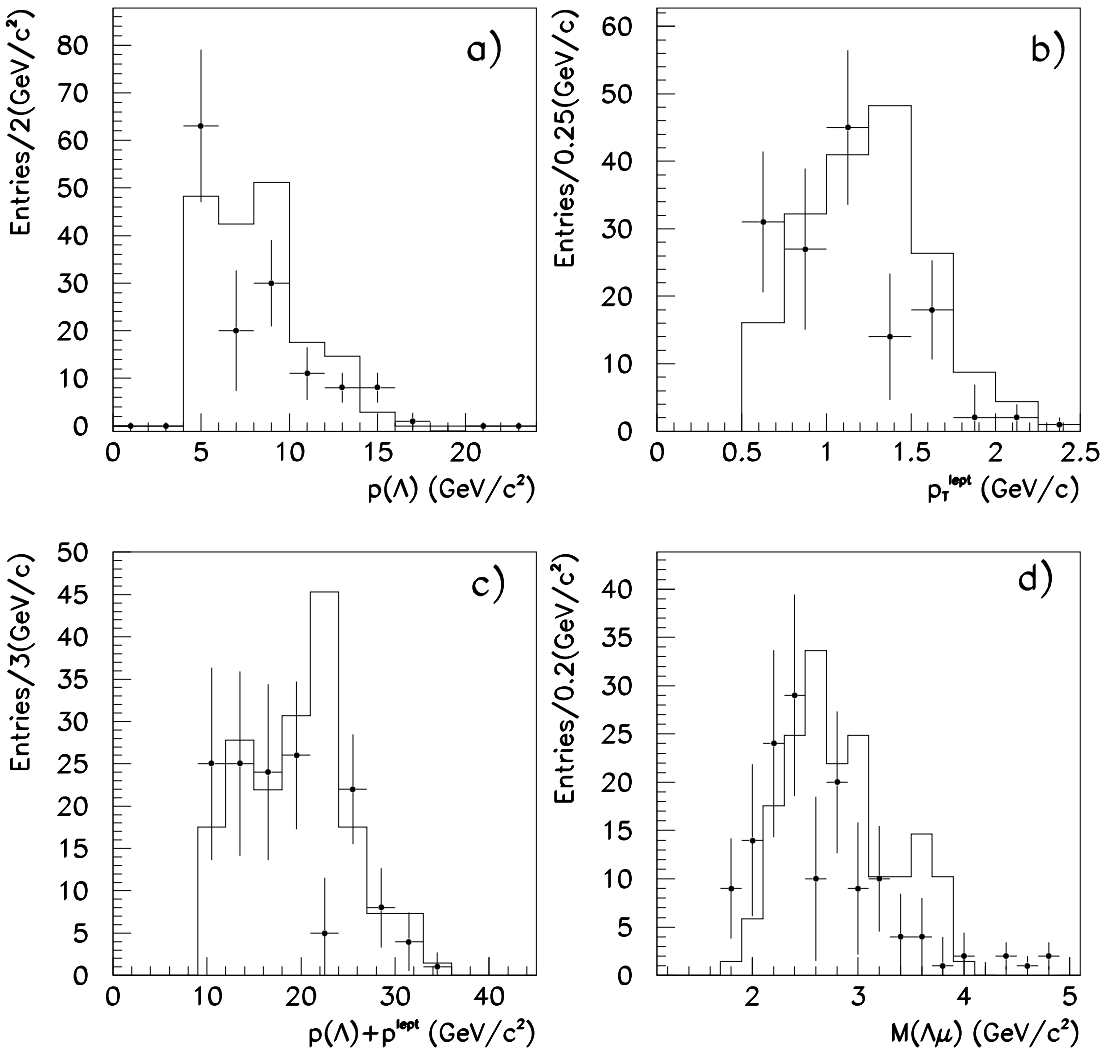

Figure 3: Subtracted spectrum (right sign - wrong sign) in the data (dots) for: a) Λ momentum, b) lepton transverse momentum, c) the sum of the Λ and lepton momenta and d) $\Lambda\ell$ invariant mass. The histograms show the simulation for the b-baryon signal.

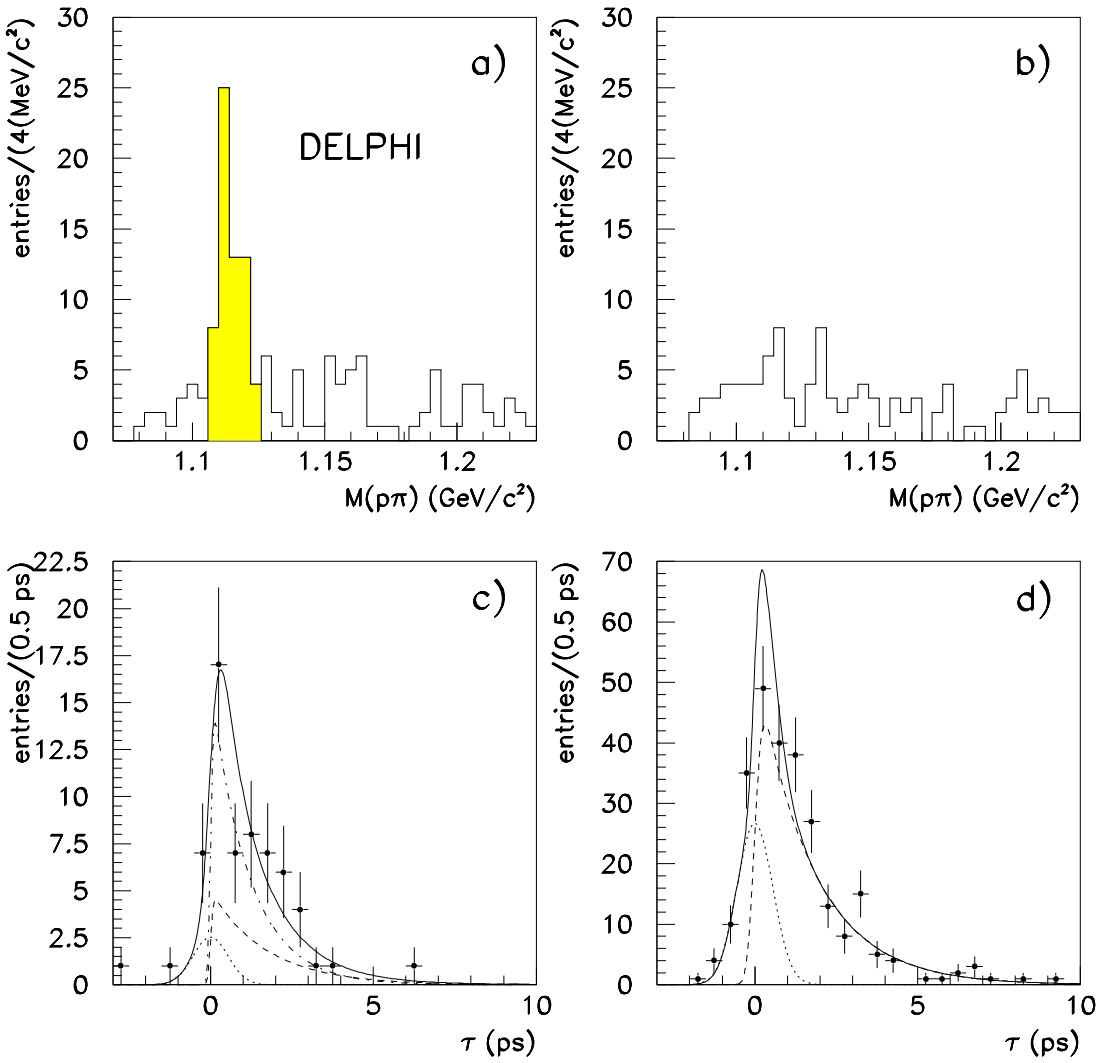

Figure 4: Λ signal for reconstructed $\Lambda\mu\pi$ vertices of a) right sign and b) wrong sign respectively; c) lifetime distribution for 63 b-baryon candidates (hatched area in the Λmass plot); the full lines represent the result of the fit described in the text; the dotted-dashed line is the estimated b-baryon contribution, the dashed and dotted lines represent the flying and not-flying background respectively, determined from d) the lifetime distribution of the background sample, $\Lambda\mu\pi$ vertices with wrong sign or $p\pi$ mass outside the above range.

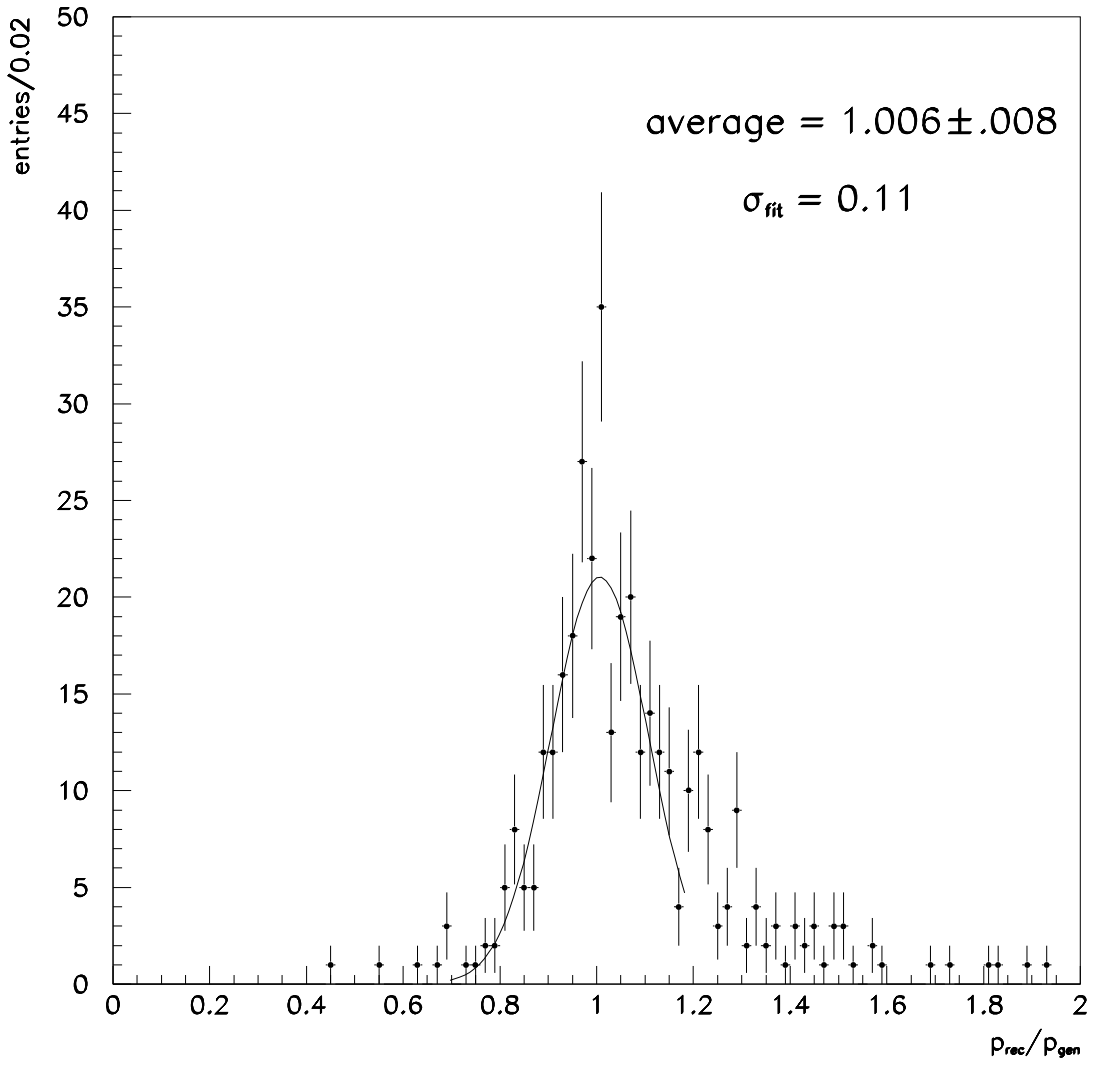

Figure 5: Ratio between estimated and generated Λ_b momentum predicted by the simulation for the decay channel $\Lambda_b \to \Lambda_c \mu \nu$. The curve is the result of a Gaussian fit to the distribution.

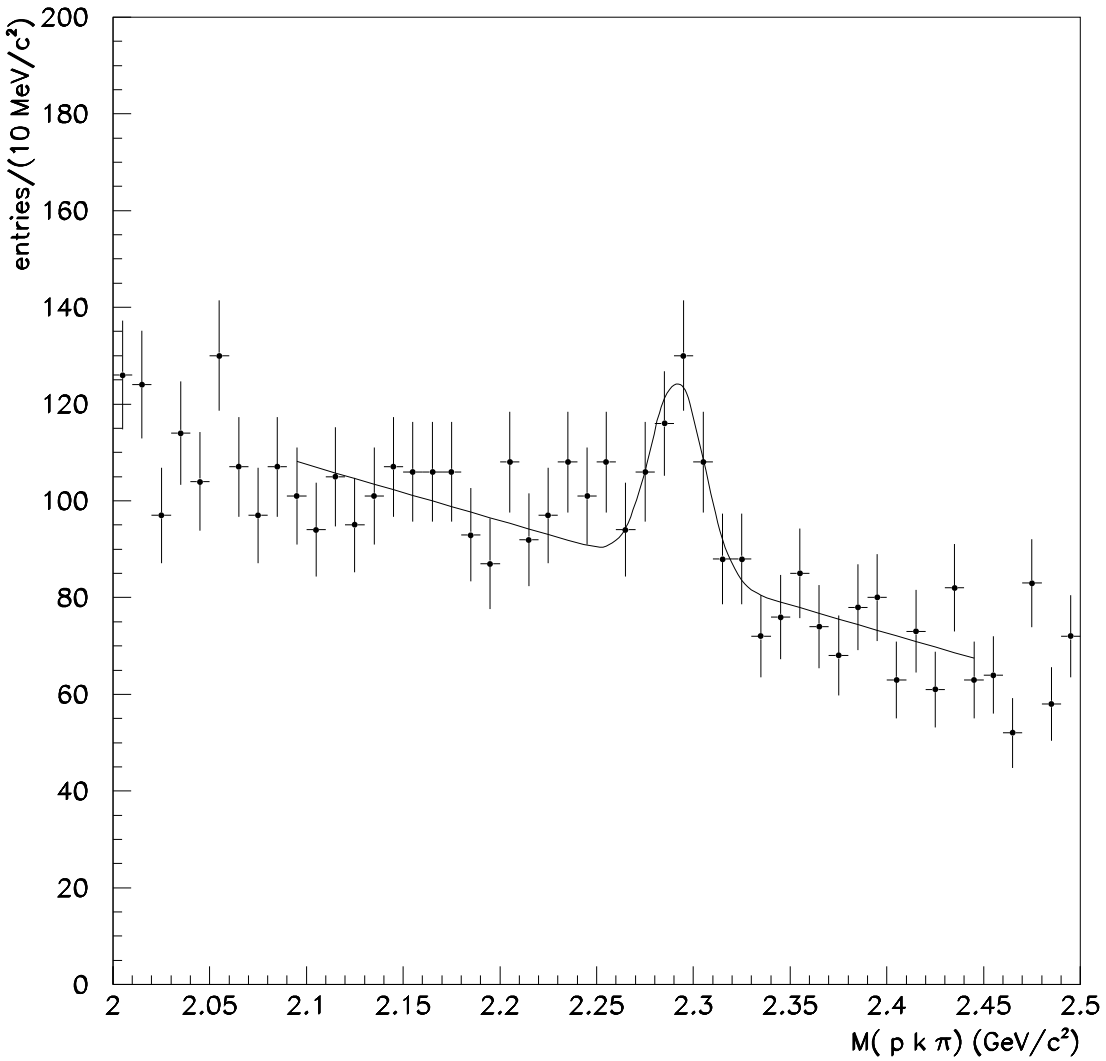

Figure 6: Λ_c inclusive signal for reconstructed $pK\pi$ vertices. The curve is the result of a fit to the distribution using a Gaussian superimposed on a linear background.

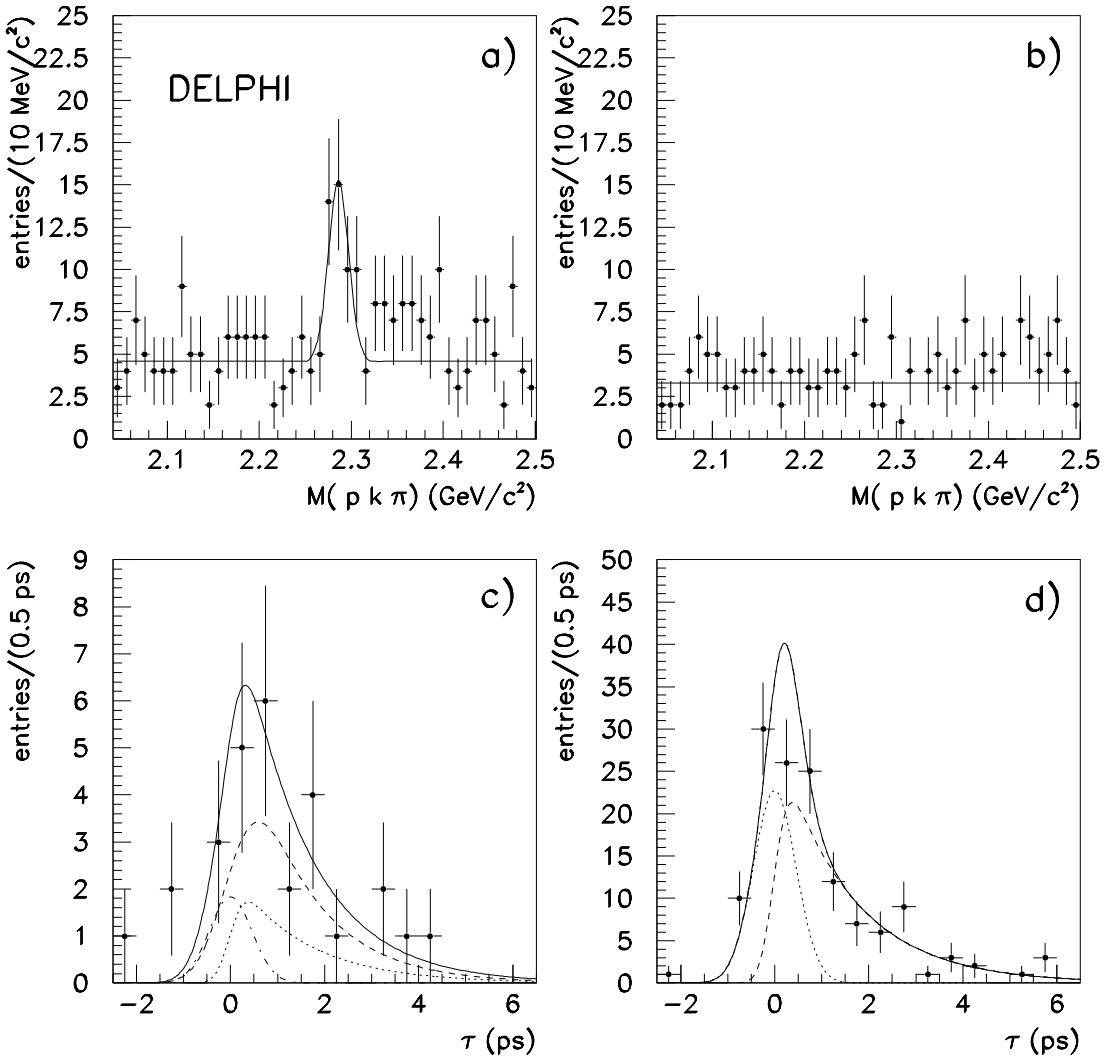

Figure 7: a,b) $pK\pi$ invariant mass distribution for $\Lambda_c\ell$ pairs of opposite sign and same sign respectively; c,d) proper time distributions for b-baryon signal and background sample. The curves are as in figure 4.

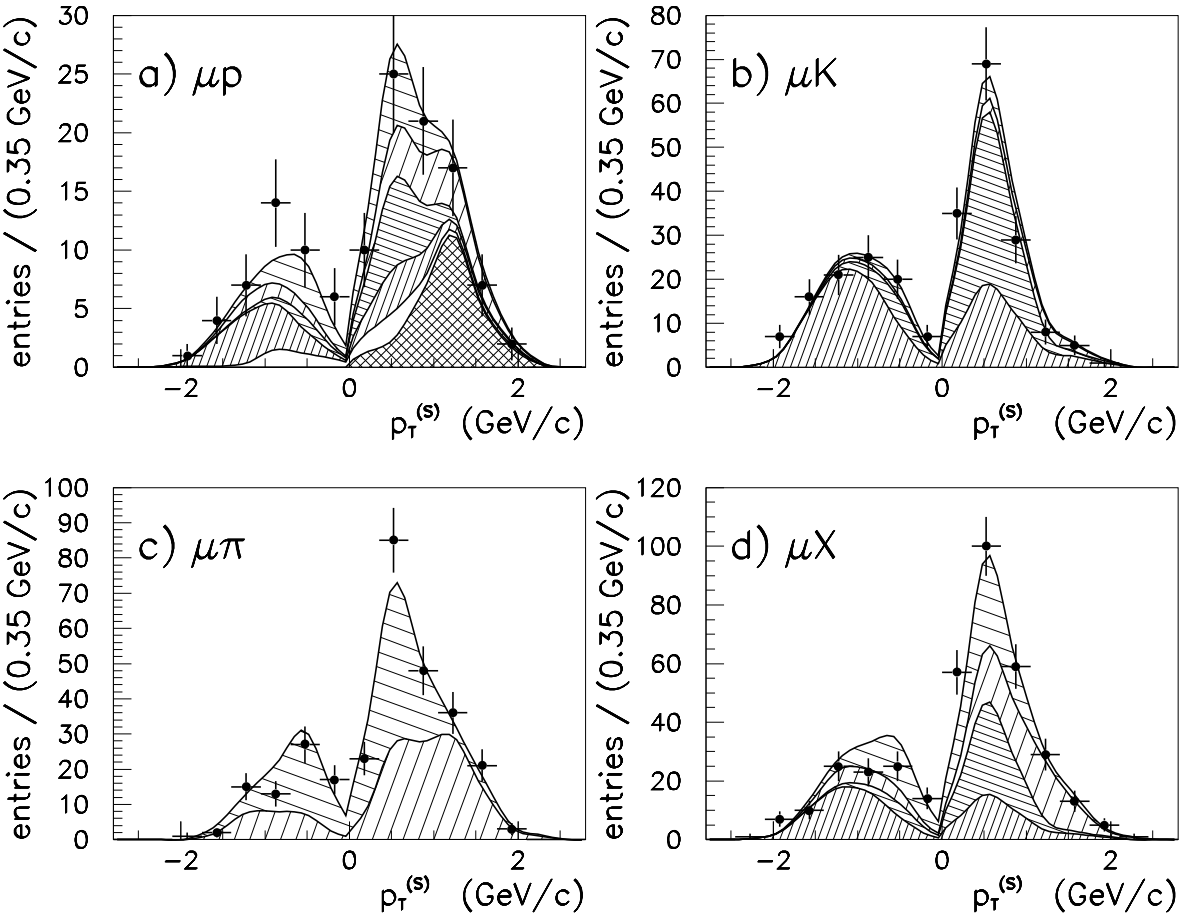

Figure 8: Projection of the data distribution onto the $p_T^{(S)}$ axis (where $p_T^{(S)}$ is signed transverse momentum of the muon. Its positive values correspond to the *right sign* combination (muon and hadron have opposite charges), whereas negative values to the *wrong sign* one (same sign μ–hadron pairs). Points with error bars (data) are compared to the fit (uppermost curve) decomposed into six classes shown with different hatching. The four plots shown correspond to the four samples used in the fit.

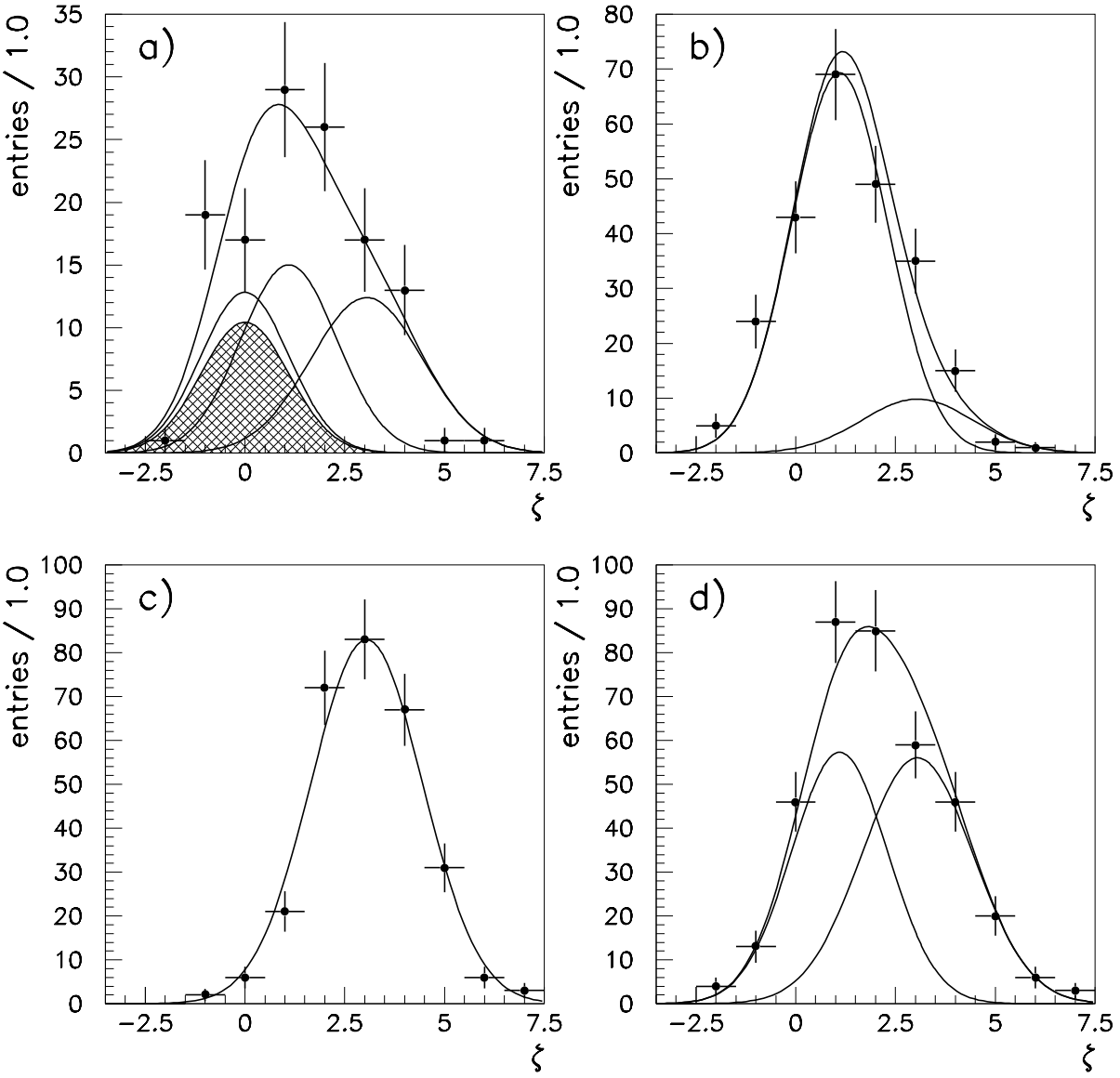

Figure 9: Projection of the data distribution onto the ζ axis. Points with error bars (data) are compared to the fit represented by the uppermost curve. This curve is the sum of the p, K, π contributions, shown with Gaussians centered at ζ = 0.0, 1.1, 3.05 respectively. The four plots correspond to the four samples used in the fit: a) μp sample (the signal content is hatched); b) μK sample; c) $\mu\pi$ sample; d) μX sample.

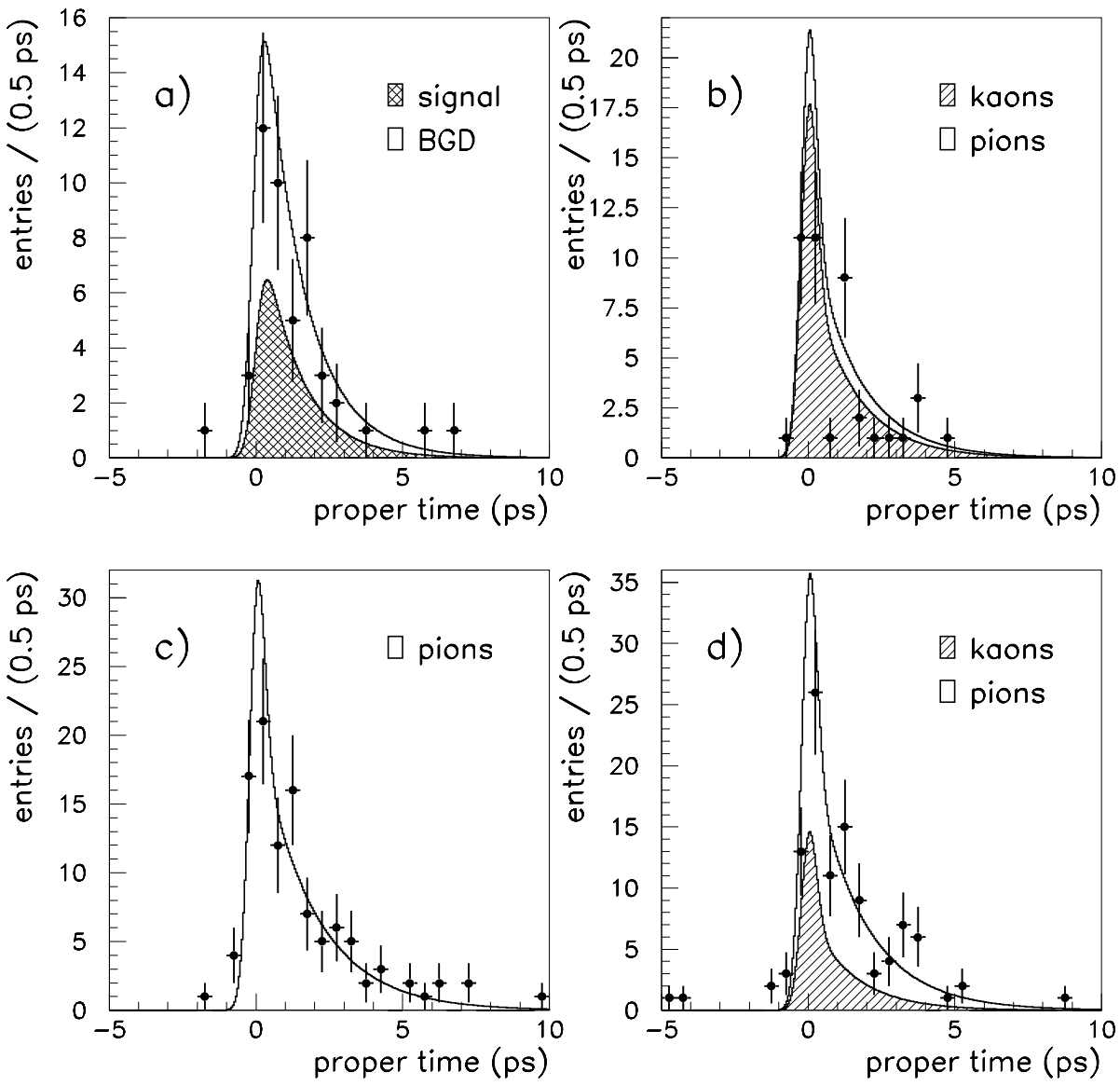

Figure 10: Projection of the data distribution onto the proper time axis for $p_T^{(S)} > 0.7\mathrm{GeV}/c$. The data are represented by points with the error bars, the fit is shown with up-most continuous lines: a) μp sample – the signal is shown double hatched; b) μK sample – the kaon content is shown single hatched; c) $\mu\pi$ sample; d) μX – the kaon content is shown single hatched.

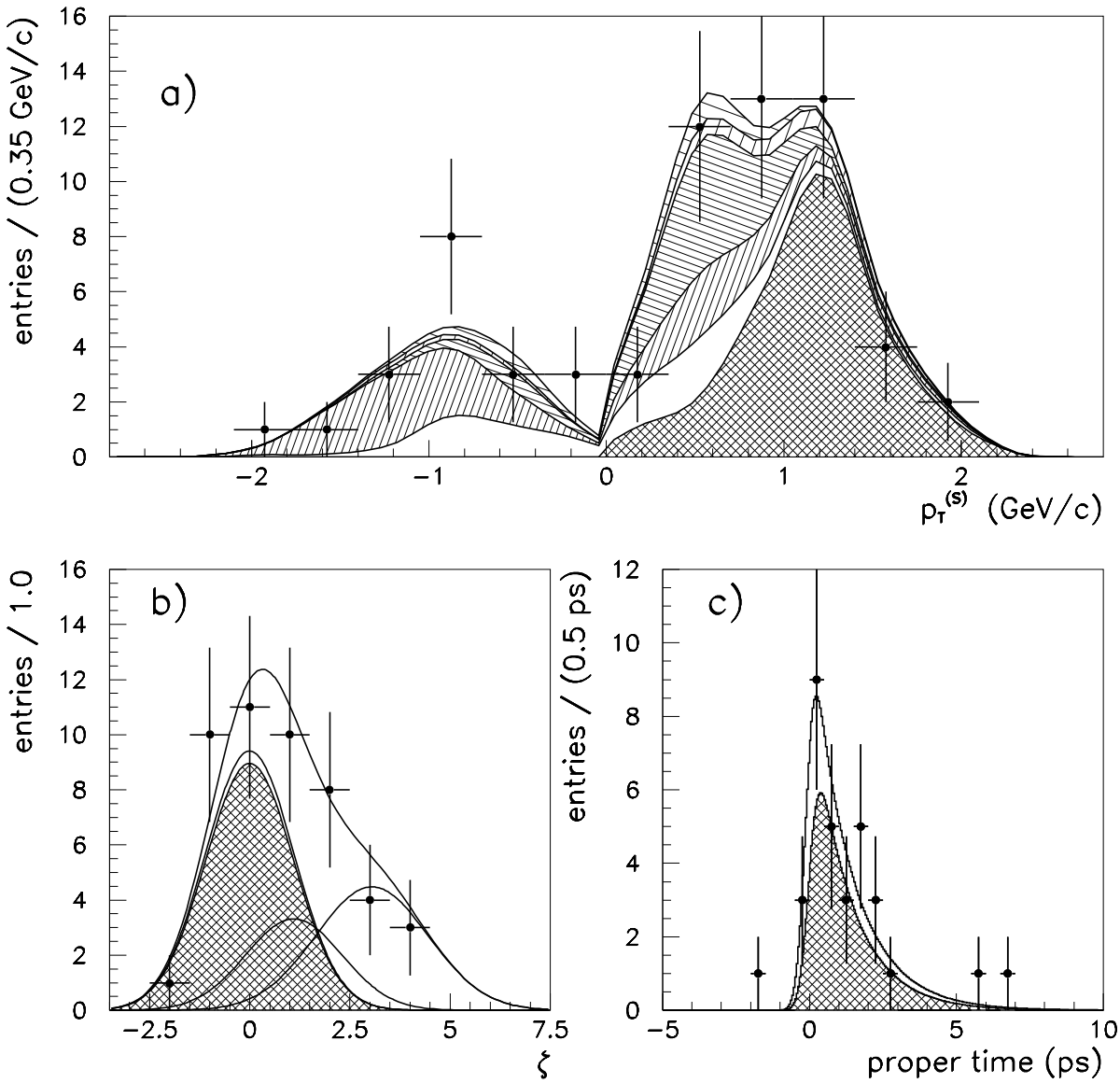

Figure 11: Projections of the μp sample onto (a) $p_T^{(S)}$ axis with a cut $\zeta < 1.5$, (b) ζ axis with a cut $p_T^{(S)} > 0.7 GeV/c$ and (c) proper time axis with both cuts applied. The signal content is shown double hatched (the hatching on the figure (a) is explained in the caption to the figure 8).

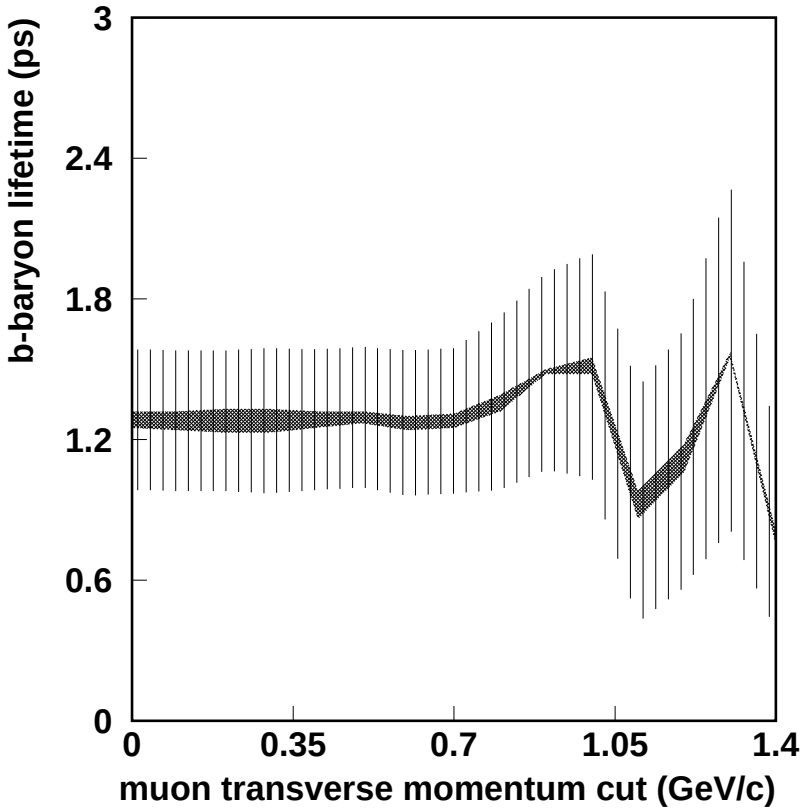

Figure 12: Study of the stability of the b-baryon lifetime determination with respect to a given muon transverse momentum cut. The width of the double hatched area shows the uncertainty due to parameterization of the proton background $\mathcal{P}_t$ effective lifetime (the lower border was obtained with the pion parameterization, the uper one with zero effective lifetime). Vertical bars shows the symmetric error of the fit.

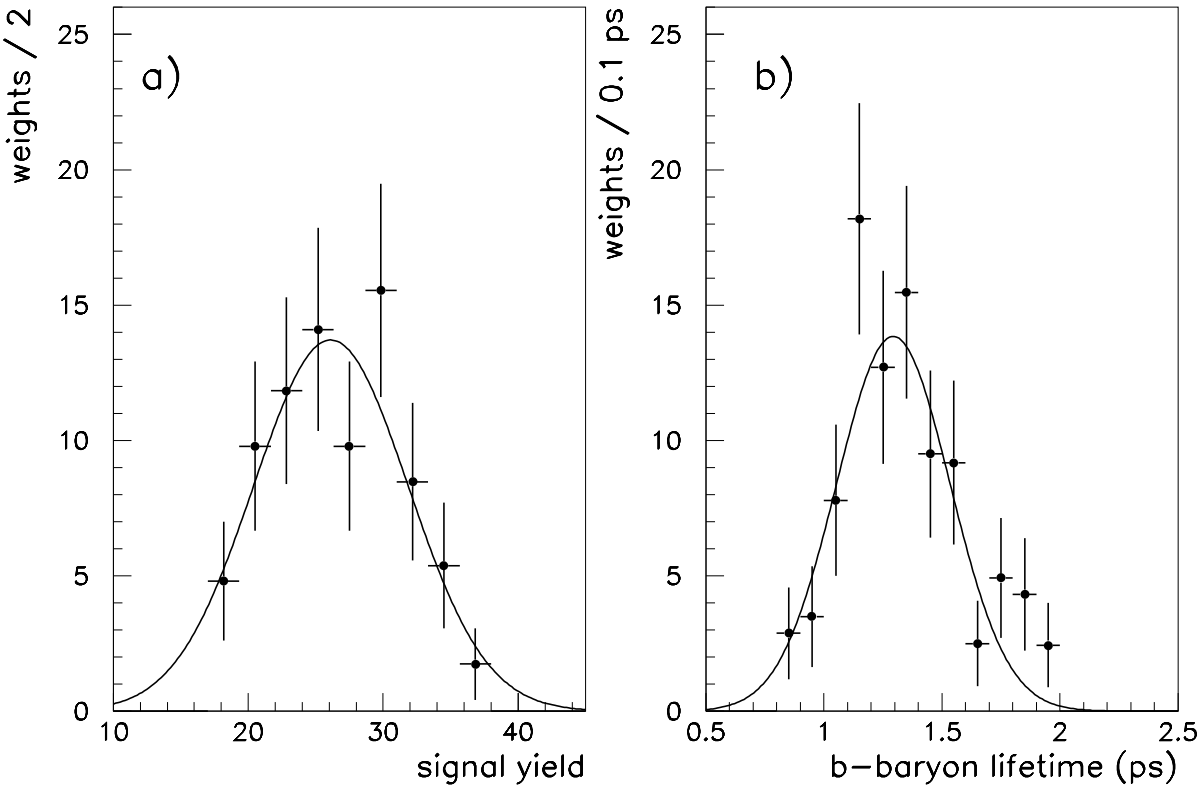

Figure 13: Results of the toy Monte Carlo simulation described in the text – points with error bars – are fitted with Gaussians for a) estimated signal yield (input value = 28, output mean value = 26, RMS = 6); b) estimated b-baryon lifetime (input value = 1.3 ps, output mean value = 1.29 ps, RMS = 0.24 ps).